Thesis

Applying optical coherence tomography angiography to evaluate potential retinal vascular alterations in pregnant women both with and without diabetes mellitus

submitted by

Sebastian Risling, B.Sc.

in partial fulfillment of the requirements for the degree of

Doktor der gesamten Heilkunde

(Dr. med. univ.)

at the

Medical University of Graz

executed at the

Department of Ophthalmology

under the supervision of

Andreas Wedrich, Univ.-Prof. Dr.med.univ.

Laura Posch-Pertl, Dr.med.univ.

Graz, April 19th, 2024

Declaration of Academic Integrity

I hereby confirm that the present diploma thesis is the result of my own independent scholarly work. I also confirm that in all cases, where material from the work of others (in books, articles, essays, dissertations, and on the internet) is acknowledged, quotations and paraphrases are clearly indicated. No material other than that cited in the reference list has been used. I have read and understood the Medical University's regulations and procedures concerning plagiarism.

Graz, April 19th, 2024 *Sebastian Risling m.p.*

Acknowledgements

Firstly, I would like to sincerely thank my supervisor, Dr.in Laura Posch-Pertl, for her constant support and guidance throughout the course of this thesis. I am also grateful to Univ.-Prof. Dr. Andreas Wedrich, for promptly scheduling meetings and providing a well-organized framework. Their supervision allowed me to work and learn in a well-supported environment throughout the entire progression of the thesis.

In addition, a special acknowledgment is owed to Dr. Wolfgang List as well as the ophthalmic technicians, especially to Lydia Helfer and Sabine Stenitzer, for their contribution to the process of data collection. I am thankful for their vigorous support on-site and the exceptional kindness they have shown.

Lastly, I would like to thank my significant other, as well as my family back home, who encouraged and inspired me throughout all phases of the project.

Zusammenfassung

Einleitung. Die Schwangerschaft gilt als eine Phase physiologischer und hämodynamischer Veränderungen mit potenziell alterierenden Auswirkungen auf das Gefäßsystem des Auges. Es ist bekannt, dass die Schwangerschaft im Falle eines vorliegenden Diabetes Mellitus das Voranschreiten der diabetischen Retinopathie begünstigen kann. Die vorliegende Pilotstudie hat das Ziel, mithilfe der Optischen Kohärenztomographie-Angiographie (OCTA) eine detailgenaue Betrachtung retinaler Gefäße vorzunehmen, um die Effekte von Schwangerschaft, präexistenziellem Diabetes Mellitus und Gestationsdiabetes auf die retinale Gefäßplexusdichte zu beurteilen.

Methoden. 20 schwangere Frauen, darunter 12 Frauen mit präexistenziellem Diabetes (PexD), 5 Frauen mit Gestationsdiabetes (GDM) und 3 Frauen ohne Diabetes Mellitus wurden mithilfe der OCTA mit einer Kontrollgruppe von 19 gesunden nichtschwangeren Frauen über zwei Messzeitpunkte hinweg verglichen, im Zeitraum der 25.- 28. Schwangerschaftswoche sowie in der 37.- 40. Woche. Untersucht wurde die Gefäßdichte des superfiziellen Gefäßplexus (SCP), des tiefen Gefäßplexus (DCP), des peripapillären Gefäßplexus (RPCP) sowie die Größe der fovealen avaskulären Zone (FAZ).

Ergebnisse. Innerhalb der gesunden Schwangeren nahm die SCP-Gefäßdichte um einen absoluten Wert von 0.40% zu, bei den Schwangeren mit PexD um 0.53% und bei den gesunden nichtschwangeren Frauen lediglich um 0.29%. Die DCP Gefäßdichte erhöhte sich um durchschnittlich 7.17% innerhalb der gesunden Schwangeren, um 1.92% innerhalb der Frauen mit PexD sowie um 0.71% innerhalb der gesunden nichtschwangeren Frauen. Während die Gefäßdichte des RPCP innerhalb der gesunden Schwangeren unverändert blieb, zeigte sich eine Abnahme um -0.50% bei den schwangeren Frauen mit PexD und um -0.42% bei den gesunden nichtschwangeren Frauen.

Diskussion. Die momentanen Daten lassen hinsichtlich der retinalen Plexusdichte einen Trend erkennen, der darauf hindeutet, dass es überwiegend zu einer Zunahme der Gefäßdichte während der Schwangerschaft kommt. Weiters erscheinen diese Veränderungen zwischen gesunden Schwangeren und schwangeren Diabetikerinnen in unterschiedlichem Maße. Um jene Unterschiede fortführend statistisch beurteilen zu können, sind in Zukunft weitere Auswertungen notwendig, die im Rahmen des Studienprojekts erfolgen werden.

Abstract

Introduction. Pregnancy is considered a period of physiological and hemodynamic changes with potentially altering effects on the vascular system of the eye. It is known that pregnancy may promote the progression of diabetic retinopathy in the presence of diabetes mellitus. The aim of this pilot study is to use optical coherence tomography angiography (OCTA) to perform a detailed examination of retinal vessels in order to assess the effects of pregnancy, preexisting diabetes mellitus and gestational diabetes mellitus on retinal capillary plexus density.

Methods. A total number of 20 pregnant, including 12 women with preexisting diabetes mellitus (PexD), 5 women with gestational diabetes mellitus (GDM), and 3 healthy pregnant women, were compared to 19 healthy non-pregnant women by using OCTA over two different times of examination throughout pregnancy. The vessel density of the superficial capillary plexus (SCP), the deep capillary plexus (DCP), and the radial peripapillary capillary plexus (RPCP), as well as the size of the foveal avascular zone (FAZ) were examined.

Results. In descriptive terms, the vessel density of the SCP increased throughout pregnancy across all groups. Regarding the whole macula, the SCP vessel density increased by an absolute value of 0.40% in healthy pregnant women, by 0.53% in women with PexD and by 0.29% in the control group. In line with these results, the DCP vessel density increased across all groups, with a mean increase of 7.17% within the healthy pregnant women, of 1.92% within the women with PexD and of 0.71% within the healthy controls. However, while no change in vessel density was observed in the healthy pregnant women regarding the RPCP vessel density, a decrease of -0.50% in the pregnant women with PexD and -0.42% in the healthy non-pregnant women was observed.

Discussion. Regarding the retinal plexus vessel density, the current data indicates a trend which suggests that there is an increase in vessel density during pregnancy. Furthermore, these changes appear to differ between healthy pregnant women and pregnant diabetics. To assess these differences more precisely, further evaluations are necessary in the future, which will be carried out as part of the ongoing study project.

Table of Content

Acknowledgements II
Zusammenfassung III
Abstract IV
Table of Content V
List of Abbreviations VII
List of Figures VIII
List of Tables IX
1. Introduction 1
1.1. The eye, its capillary plexus, and the foveal avascular zone 1
1.1.1. The retina: Microstructure and segmentation 1
1.1.2. Choroidal architecture 4
1.1.3. Microvasculature in detail: Retinal and choroidal perfusion 4
1.2. Diabetes mellitus 9
1.2.1. Clinical types of diabetes mellitus and their prevalence 10
1.2.2. Clinical features and effects on human microvasculature 13
1.2.3. Diabetic retinopathy 14
1.2.4. Diabetic macular edema 18
1.3. Imaging techniques for retinal vasculature 18
1.3.1. Fluorescein angiography 19
1.3.2. Optical coherence tomography 21
1.3.3. Optical coherence tomography angiography 22
1.4. Pregnancy, diabetes and their impact on the eye's vascular system 26
1.5. Current literature: Insights and discrepancies 27
1.6. Study aims, rationale and hypotheses 29
2. Material and Methods 30
2.1. Sample, patient recruitment, inclusion criteria, exclusion criteria 30
2.2. Patient examinations 30
2.3. Ophthalmological examination and image acquisition 31
2.4. Study design, variables and statistical analyses 33
3. Results 35
3.1. Demographics 35
3.2. Results of ophthalmological examination 36
3.2.1. Retinal thickness 37
3.2.2. Choroidal thickness 38

3.2.3. Retinal Nerve Fiber Layer (RNFL) thickness 39
3.2.4. Retinal vessel density: Superficial Capillary Plexus (SCP) 40
3.2.5. Retinal vessel density: Deep Capillary Plexus (DCP) 42
3.2.6. Small vessel density: Peripapillary Capillary Plexus (RPCP) 45
3.2.7. Foveal Avascular Zone (FAZ) size 46
4. Discussion 48
References 52

List of Abbreviations

ADA … American Diabetes Association
BRB … Blood retinal barrier
DCP … Deep capillary plexus
… Also referred to as Deep vascular plexus DVP
D … Diopters
DME … Diabetic macula edema
DR … Diabetic retinopathy
FA … Fluorescein angiography
FAZ … Foveal avascular zone
GCL … Ganglion cell layer
GCT … Glucose Challenge Test
GDA … German Diabetes Association
GDM … Gestational Diabetes Mellitus
ICA … Internal carotid artery
IPL … Inner plexiform layer
ICP … Intermediate capillary plexus
… Also referred to as Intermediate vascular plexus IVP
ILM … Internal limiting membrane
LPCA … Long posterior ciliary arteries
NPDR … Non-proliferative diabetic retinopathy
NVD … Neovascularization of the disc
NVE … Neovascularization elsewhere
OCT … Optical coherence tomography
OCTA … Optical coherence tomography angiography
oGTT … Oral glucose tolerance test
ONL … Outer nuclear layer
PDR … Proliferative diabetic retinopathy
PexD … Preexisting Diabetes Mellitus, Pregestational Diabetes Mellitus
PR … Photoreceptor layer
RNFL … (Retinal) Nerve fiber layer
RPC … Radial peripapillary capillaries
… Also referred to as Radial peripapillary capillary plexus RPCP
RPE … Retinal pigment epithelium
SCP … Superficial capillary plexus
… Also referred to as Superficial vascular plexus SVP
SPCA … Short posterior ciliary arteries
VEGF … Vascular endothelial growth factor

List of Figures

Figure 1. *Subdivision of the macula lutea.*
(Adapted from Yanoff & Duker, 2019, p. 421) 2
Figure 2. *Retinal Fluorescein Angiography*.
(Reprinted from Böhm, 2019, p. 4) 6
Figure 3. *Retinal layers with visualization of the different vascular plexus.*
(Reprinted from Böhm, F., 2019, p. 5) 7
Figure 4. *Peripapillary vascular architecture.*
(Reprinted from Schmetterer & Kiel, 2012, p. 18) 8
Figure 5. *Imaging characteristics of fluorescein angiography.*
(Reprinted from UIHC Department of Ophthalmology, 2022) 24
Figure 6. *Imaging characteristics of OCTA.*
(Reprinted from O'Keefe, Ghazala D., 2022) 24
Figure 7. *Subdivision of macula and optic disc in further areas by OCTA.*
(Own illustration captured in RTVue XR Avanti, 2023) 33
Figure 8. *Mean SCP vessel density for whole macula (in %) considering both eyes collectively across all four groups at baseline and at follow-up visits*. 41
Figure 9. *Mean SCP vessel density for fovea (in %) considering both eyes collectively across all four groups at baseline and at follow-up visits.* 41
Figure 10. *Mean DCP vessel density for whole macula (in %) considering both eyes collectively across all four groups at baseline and at follow-up visits*. 43
Figure 11. *Mean DCP vessel density for fovea (in %) considering both eyes collectively across all four groups at baseline and at follow-up visits.* 44
Figure 12. *Mean RPCP vessel density (in %) considering both eyes collectively across all four groups at baseline and at follow-up visits*. 45

List of Tables

Table 1. *Study schedule including perfomred testing and imaging for the pregnant and non-pregnant women each at baseline and follow-up visits* 31
Table 2. *Demographic data including age, spherical equivalent, body mass index and blood glucose levels for all four study groups* 36
Table 3. *Mean retinal thickness across all study groups considering both eyes collectively at baseline and follow-up visit* 37
Table 4. *Mean choroidal thickness across all study groups considering both eyes collectively at baseline and follow-up visit* 38
Table 5. *Mean RNFL thickness across all study groups considering both eyes collectively at baseline and follow-up visit* 39
Table 6. *Mean vessel density of the superficial capillary plexus across all study groups considering both eyes collectively at baseline and follow-up visit* 42
Table 7. *Mean vessel density of the deep capillary plexus in percent across all study groups considering both eyes collectively at baseline and follow-up visit* 44
Table 8. *Mean vessel density of the radial peripapillary capillary plexus in percent across all study groups considering both eyes collectively at baseline and follow-up visit* 46
Table 9. *Mean size of the foveal avascular zone in mm2 across all study groups considering both eyes collectively at baseline and follow-up visit* 47

1. Introduction

According to previous research, pregnancy, accompanied by constant hormonal and physiological changes, as well as metabolic disorders such as diabetes mellitus, do affect even smallest vessels in several tissues. With the help of well-established ophthalmic imaging devices such as fluorescein angiography, it has become technically possible to examine the ophthalmic microvasculature to a reasonable extent and to further evaluate the effects of said metabolic changes or impairments. With the implementation of optical coherence tomography angiography (OCTA), an even more accurate level of detail has been made accessible to examine, which made it possible to visualize and monitor retinal and choroidal microvasculature in high-resolution detail. Although there has been a considerable amount of research regarding pregnancy, diabetes mellitus, and their effects on retinal microvasculature over the last few years, different results remain conflicting. While certain researchers observed a homogeneous change in vascular density within the different retinal plexuses, data obtained in other studies suggested much smaller effects, or even opposing results. Therefore, further research remains necessary.

The current thesis attempts to address and reassess said matter by taking into account previous limitations already discussed by other authors, as well as potential shortcomings. Overall, it is designed to be a precursor and interim evaluation, preceding the structurally equivalent study conducted on the same data gathered over a longer period of time. Before eventually discussing previous research and deriving current hypotheses, the following chapters will provide an overview of the anatomical and microvascular structure of the posterior segment of the eye, the functionality and applicability of current imaging techniques for visualization of retinal microvasculature, and the effect of different types of diabetes mellitus, as well as pregnancy on the structure and density of retinal vasculature.

1.1. The eye, its capillary plexus, and the foveal avascular zone

Before further addressing the topics of diabetic retinopathy, current ophthalmologic imaging modalities, pregnancy, and their actual interdependency, it may be helpful to recall the anatomical and microstructural features of the posterior eye segments, focusing on the retina, the choroid, the optic nerve, and associated vasculature, in advance.

1.1.1. The retina: Microstructure and segmentation

As an evolutionary sensory part of the central nervous system, the retina is markedly responsible for the physical detection and chemical conversion of light and its neural

transmission to the visual cortex (Yanoff & Duker, 2019:29). The retina therefore represents an integral, indispensable facet of vision, that enables to perceive visual stimuli on a daily basis.

Anatomically, it can be divided into two major planar sections and various vertical microlayers. Regarding the planar segmentation, posteriorly located is the Pars Optica Retinae, designated as the 'neural retina' (Yanoff & Duker, 2019:419). This transparent retinal section warrants the everyday visual perception with the integrity of photoreceptor cells and additional associated stimuli-processing neuronal layers. Anteriorly, separated by the Ora Serrata, approximately 9mm posterior of the corneal limbus, the Pars Optica Retinae merges into the Pars Caeca Retinae. This section anatomically joins the pigmented as well as the nonpigmented epithelium of the ciliary body and the iris and, in contrast to the neural retina, is not capable of detecting visual stimuli due to its lack of receptor cells (Yanoff & Duker, 2019:419).

Focally located amid the posterior neural retina is the elliptical macula lutea. This 3mm diameter sized area is where the incident light, following the optical axis, impinges at, after pervading the anterior ophthalmic sections and the vitreous (Yanoff & Duker, 2019:29). Going further into detail, the macula itself can be subdivided into several, cockade-shaped areas: The perifovea, as the outermost ring-shaped area, the parafovea, the fovea, the foveola and the umbo, representing the most central point of the macula (Yanoff & Duker, 2019:421). The macular cockade is illustrated in figure 1.

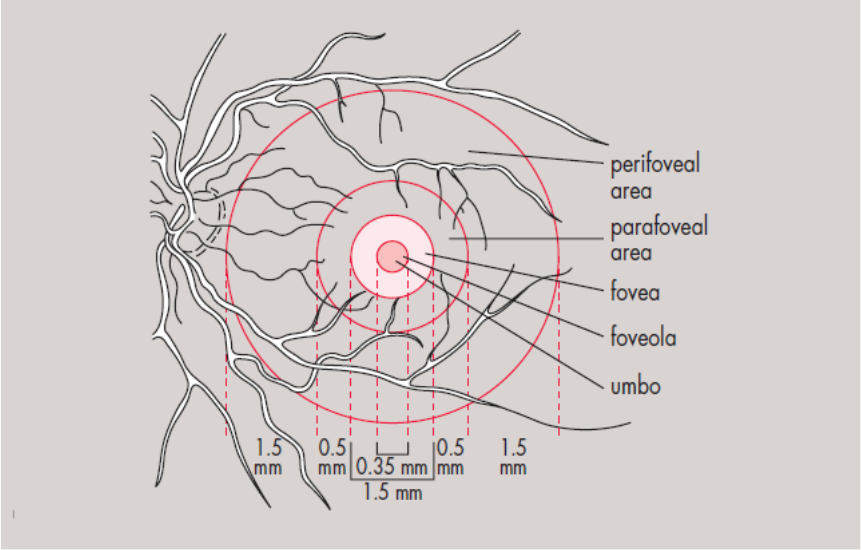

Figure 1. Subdivision of the macula lutea. (Left eye) Subdivision into several cockade-shaped sections, with their dimensioning and size being illustrated in contrast to the surrounding branch arteries. (Adapted from Yanoff & Duker, 2019, p. 421)

The perifovea represents the outlying, 1.5mm diameter wide region that functionally contains mainly ganglion cells, bipolar cells, and nerve fibers. Further inwards, the 0.5mm diameter wide parafovea follows, which too is largely composed of ganglion cells, bipolar cells, and nerves fibers, analogous to the surrounding perifovea. Proceeding further towards the center, the fovea centralis retinae is located, measuring 1.5mm in diameter. Unlike the rest of the outer retina, its neural cells follow a so-called lateral displacement, ensuring undisturbed perception of incident light (Yanoff & Duker, 2019:420). The fovea itself is a predominantly avascular, excavated area, containing cone-cells. In its center, the foveola with a diameter of 350µm is surrounding the umbo, densely containing cone cells. The umbo, as a 150-200µm diameter sized spot, contains the maximum density of photoreceptor cells along the entire retina and is provided exclusively with type-M and type-L cone cells, often referred to as 'central bouquet of cones' enabling the highest visual acuity in the neural retina (Yanoff & Duker, 2019:420; Grehn, 2019:12; Gervasio & Peck, 2022).

In addition to its planar organization, the neural retina can be also subdivided into several successive layers containing various neural cells and nerve fibers (Yanoff & Duker, 2019:421; Grehn, 2019:12). The innermost of these layers, the internal limiting membrane (ILM), separates the retina directly from the vitreous.

On a side note, anatomically-segmentally speaking of 'inner side, to outer side' refers to the inner retinal side featured by the ILM and the outer side featured by the retinal pigment epithelium (RPE), further facing the Bruch's membrane. The cell bodies of the receptor cells are located in the Outer Nuclear Layer (ONL). Still, following outwards, their cones and rods segments located in the Photoreceptor Layer (PR) are protruding into the RPE (Yanoff & Duker, 2019:422). Inside the RPE, numerous melanosomes are responsible for its mixed pigmentation, which serves as a 'light filter' to absorb scattered light. Furthermore, the RPE assists maintaining the nourishment and the immunological assistance of the overlying photoreceptor cells (Yanoff & Duker, 2019:423).

Bilateral nasally to the fovea, the optic papilla represents the exit point of the optic nerve, consisting of the totality of individual ganglion cell nerve fibers, ranging through the nerve fiber layer of the inner retina. It also represents the entry-point of various vessels, discussed further below, as well as innervating nerves. Since the optic disc does not hold photoreceptor cells, it is referred to as 'blind' spot (Yanoff & Duker, 2019:875; Grehn, 2019:12).

1.1.2. Choroidal architecture

The choroid, as a highly vascularized membrane and posterior part of the uvea, is located in between the retina and the sclera. It is responsible for maintaining the outer retinal homeostasis. This homeostasis involves the maintenance of the retina's vascular supply and nourishment, the absorption of light, and the modulation of intraocular pressure by applying a vasomotor control of blood flow (Yanoff & Duker, 2019:426). In addition, the choroid also monitors thermoregulation: Because heat is generated during the photochemical reactions, energy must be drawn off (Grehn, 2019:12).

Histologically, analogous to the retina, the choroidal microstructure can be further segmented into multiple layers, with the most inner one, bordering the retina, being the Bruch's membrane (Yanoff & Duker, 2019:426; Grehn, 2019:11).

1) The Bruch's membrane mostly consists of elastic fibers and collagen fibers and is directly apposing the RPE lying above. Moreover, it is involved in the formation and the maintenance of the blood-retinal barrier.

2) The choriocapillaris, a 7 – 10µm thick network containing the patch-like patterned fenestrated choroidal capillaries, maintaining the abovementioned outer retinal blood supply, described below (Yanoff & Duker, 2019:426).

3) The lamina vasculosa, further being divided into the Sattler's layer as well as the Haller's layer, with both containing arterioles, small arteries and veins. The Sattler's layer is particularly warranting the choriocapillaris blood flow and is furthermore involved in immunological defense, by containing mast cells, macrophages, and lymphocytes. (Yanoff & Duker, 2019:427).

4) The lamina suprachoroidea, as a transitional zone between the choroid and the sclera, consisting of elastic fiber tissue (Yanoff & Duker, 2019:426; Schmetterer & Kiel, 2012:10).

The entirety of the retina and choroid along with their different layers and neural cells requires a reliably maintained and precisely targeted blood supply. This will be elaborated in the following chapter.

1.1.3. Microvasculature in detail: Retinal and choroidal perfusion

The blood supply of the posterior eye segments is complex and is provided by a variety of vascular branches originating from the ophthalmic artery at different locations. Overall, the retinal as well as the choroidal vessels share the supply and nourishment of the corresponding structures. The inner two thirds of the retina are supplied by retinal vessels

themselves, while the outer third of the retina, including the photoreceptor cells and the RPE, is supplied by choroidal vessels by diffusion (Schmetterer & Kiel, 2012:174; Yanoff & Duker, 2019:426, Campbell et al., 2017:1). The ophthalmic artery itself originates from the internal carotid artery (ICA), shortly after the ICA has passed the cavernous sinus and entered the subarachnoid space (Werner et al., 2019:3). It then accompanies the optic nerve, both passing the optic canal into the orbit, where the artery continues along the medial orbit. Here it yields various arterial branches: The major branch, the central retinal artery, contains nearly 20% of the ocular blood and originates from the ophthalmic artery near the posterior side of the bulb (Schmetterer & Kiel, 2012:17). It immediately medially penetrates the optic nerve and runs midst through it, entering the eye through the papilla and gaining access to the retina (Schmetterer & Kiel, 2012:17; Werner et al, 2019:3). In parallel, the retinal venal blood drainage is warranted by the central retinal vein, running nasal to the central retinal artery through the optic nerve.

Right after exiting the optic nerve near the optic disc, the central retinal artery branches into a superior and an inferior papillary branch. These each further divide into a temporal and a nasal quadratic branch (Schmetterer & Kiel, 2012:17, Yanoff & Duker, 2019:426). As illustrated in figure 2, the two large temporal branch arteries and their accompanying veins, all running in the nerve fiber layer (NFL, often referred to as ‘retinal’ nerve fiber layer: RNFL) of the retina, arc superior as well as inferior of the macula (Yanoff & Duker, 2019:426). The two major nasal branch arteries (superior/inferior) are similarly arcuate, but much shorter. This exact vascular layout ensures that each retinal quadrant is supplied and drained by its own branch artery and vein, with the arteries typically being located anterior of the veins. Additionally, single, small arterioles, originating the central retinal artery at various intersections, run directly from the optic nerve towards the macula.

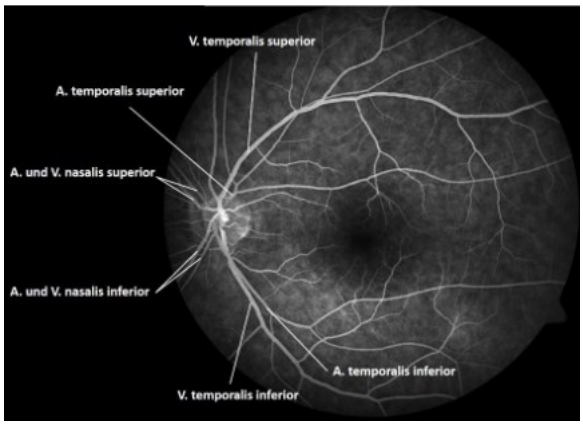

Figure 2. Retinal Fluorescein Angiography. The four branch arteries and veins supplying and draining the four retinal quadrants. (Reprinted from Böhm, 2019, p. 4)

Overall, the retinal vascular system is organized following a so-called 'end-arterial hierarchy' (Schmetterer & Kiel, 2012:17). This implies, that the beforementioned single artery branches do not yield in further specialized vessels, but instead proceed from major arteries to arterioles to the 3.5 to 6µm diameter sized capillaries, back to venules and to the major draining veins. The retinal venal blood drainage is warranted by the central retinal vein, running nasal in parallel to the central retinal artery, further draining into the superior ophthalmic vein (Grehn, 2019:13).

With the major branch arteries surrounding the macula like an arc, the inner central macula itself is devoid of retinal capillaries and is therefore vessel-free. This 400–500µm diameter avascular area is referred to as the foveal avascular zone (FAZ) (Linderman et. al, 2017:1; Yanoff & Duker, 2019:426; Schmetterer & Kiel, 2012:17). Due to the regularity with which the retinal vessels are affected by disease, their integrity became an indispensable diagnostic criterion. In this context, the FAZ can provide further orientation, as it has become the subject of interest in numerous research dealing with vascular diseases, such as diabetic retinopathy, especially since the recent use of modern microvascular imaging provided by OCTA. A more detailed insight on current relevance of FAZ imaging is given in Chapter 1.3.

Regarding the retinal microstructural layering, the retinal vasculature can be segmented into further interconnected plexuses. The uppermost plexus, the so-called superficial vascular plexus (SVP) contains larger arteries, veins, arterioles, and venules. It is primarily located inside the ganglion cell layer (GCL) and parts of the inner plexiform layer (IPL) of the retina (Campbell et al., 2017:1; Harris et al., 2020; Werner et al, 2019:4; BVA,

2017:3). Directly underneath the inner nuclear retinal layer (INL), the deep capillary plexus (DCP) is located, containing the reticular meshed, fenestrated capillaries and venules supplied by vertical anastomoses from the SVP (Campbell et al., 2017:1). According to Campbell et al. (2017), right above the INL, respectively, between the inner plexiform layer and the inner nuclear layer, the intermediate capillary plexus (ICP) is located. Although this vascular plexus has been identified anatomically, it is often grouped with the DCP in current literature and OCTA-classifications. Furthermore, current OCTA-classifications commonly merge the SVP, running in the GCL and parts of the IPL, as well as the RNFL to form an artificially joint vascular network known as the superficial capillary plexus (SCP) (Campbell et al., 2017:1). This is also the case for the present thesis.

The outer retinal layer, as mentioned above, containing the photoreceptor segments, as well as the RPE are avascular, because of their nourishment being maintained by the choriocapillaris (BVA, 2017:3; Yanoff & Duker, 2019:426, Werner et al, 2019:4). This entire vascular organization is illustrated in figure 3, which was originally created by Campbell et al. (2017, p. 2) and adapted by Böhm, F. (2019, p.5).

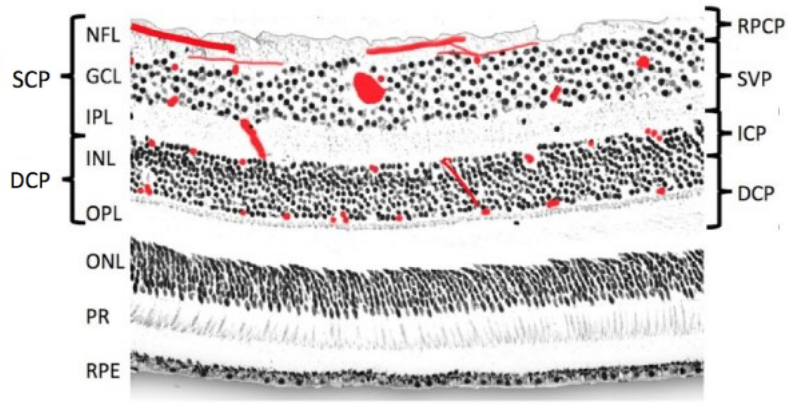

SCL = superficial capillary layer
DCL = deep capillary layer
NFL = nerve fiber layer
GCL = ganglion cell layer
IPL = inner plexiform layer
INL = inner nuclear layer
OPL = outer plexiform layer
ONL = outer nuclear layer
PR = photoreceptor layer
RPE = retinal pigment epithelium
RPCP = radial perip. capillary plexus
SVP = superficial vascular plexus
ICP = intermediate vascular plexus
DCP = deep capillary plexus

Figure 3. Retinal layers with visualization of the different vascular plexus. Left side: Retinal layers and segmentation according to OCTA. Right side: Anatomical representation of the plexuses. (Reprinted from Böhm, F., 2019, p. 5)

As the retina is its thickest around the optic disc, it is supplied by an additional particular peripapillary vascular network, whose architecture deviates from the usual bilayered meshwork consisting of SCP and DCP (Harris et al., 2020:4, Schmetterer & Kiel, 2012:18). This vascular network surrounds the papilla in a range of approximately 7.6mm from the edge of the optic disc (Mase et al., 2016, Harris et al., 2020:4). More precisely, the peripapillary vascular network is segmented into three layers, with an additional

capillary network, called the radial peripapillary capillaries (RPCs), being directly located in the superficial portion of the peripapillary RNFL (Schmetterer & Kiel, 2012:18). Figure 4 illustrates this vascular arrangement.

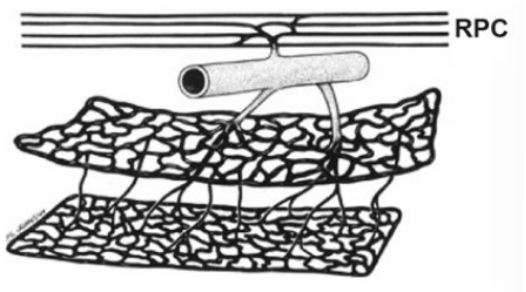

Figure 4. Peripapillary vascular architecture. The RPCs located on top, as well as the SCP and DCP below, originating from a retinal branch artery. (Reprinted from Schmetterer & Kiel, 2012, p. 18)

In contrast to the usual reticular arrangement of the retinal capillary plexuses, the RPCs run in a rectilinear pattern in parallel with the RNFL axons and rarely anastomose (Campbell et al., 2017:1). As the axons of the entire retina converge within the respective nerve fiber layer and bundle to form the optic nerve, an additional capillary network may be essential to ensure the blood supply of said fibers. A therefore interesting finding is the RPCP density correlating significantly with the thickness of the retinal nerve fiber layer (RNFL), which might confirm this assumption (Mase et al., 2016).

The choroidal blood supply, ensuring nourishment and immunological assistance of the choroid as well as the outer retinal third reaching up to the outer plexiform layer, is predominantly provided by a cluster of three major arteries: The long posterior ciliary arteries (LPCAs), the short posterior ciliary arteries (SPCAs), and the anterior ciliary arteries (Schmetterer & Kiel, 2012:11-12; Yanoff & Duker, 2019:426). These vessels all originate from the ophthalmic artery outside the bulb near the optic nerve and then penetrate the sclera at different locations. The LPCAs, after passing through the sclera, run rostral in midst the suprachoroidal space in between sclera and the choroid. Near the ora serrata, they yield additional branches, traversing back posteriorly, providing blood supply of the anterior choroid up to the equator. The SPCAs enter the choroid close to the optic nerve and provide the blood supply of the posterior choroid, reaching from the equator further posterior. They particularly maintain blood supply of the choriocapillaris, the outer parts of the optic disc, and the optic nerve. The anterior ciliary arteries penetrate the anterior sclera and send back 8 – 12 traversing branches to the outer choroid (Schmetterer

& Kiel, 2012:12). All these vessels strongly cluster and anastomose via arterioles, in threes they provide blood supply to the entire choroid, including the choriocapillaris. Venous drainage is acquired by four to six vortex veins, which further drain via the superior and the inferior ophthalmic veins (Schmetterer & Kiel, 2012:12).

The retina's homeostatic maintenance is broadly assisted by an indispensable structural array, the blood-retinal barrier (BRB). This functional barrier ensures the previously described physiologic supply of the retinal tissue and ensures the directional exchange of metabolites as well as the removal of metabolic waste between the tissue and the vascular system. (Yanoff & Duker, 2019:427). Due to the multivariate vascular microstructure of the posterior eye segment and the retinal layering, an inner BRB is to be distinguished from an outer BRB. The inner BRB is formed by tight-junctions and adherens junctions of the retinal vascular endothelium and encompassed with various retinal glia cells and pericytes. In this context, tight junctions are responsible for fencing macromolecules such as certain lipids and proteins. Additionally directional transport of macromolecules is actively managed and provided actively. For a closer understanding of major microvascular related pathophysiological mechanisms, it is important to mention that retinal capillaries are highly impermeable, even for small particles like sodium. The outer BRB is formed by tight junctions between the RPE cells. It ensures a selective permeable filtering capacity against the fenestrated capillaries of the highly vascularized choroid and maintains a controlled fluid and molecule movement between retina and choroid (Yanoff & Duker, 2019:428).

1.2. Diabetes mellitus

According to the International Diabetes Federation, there were approximately 537 million adults between the age of 20 to 79 living with diabetes in 2021 worldwide. Alarmingly, the amount of people affected by diabetes is projected to rise to roughly 643 million by 2030 and may rise even further to 783 million by 2045 worldwide. In 2021, diabetes was said to be responsible for approximately 6.7 million deaths while causing 966 billion dollars in health expenditures worldwide (IDF Atlas 10th, 2022:33). Undoubtedly, diabetes has become one of the most relevant metabolic disorders. The following chapter serves to elaborate this circumstance and furthermore discusses the manifold interrelations between diabetes mellitus and the vascular system of the eye.

1.2.1. Clinical types of diabetes mellitus and their prevalence

According to the latest guidelines for clinical practice published by the German Diabetes Association (GDA) in 2022 and the International Diabetes Guidelines published by the American Diabetes Association (ADA) in 2020, diabetes mellitus is seen as a collective term for multiple heterogeneous metabolic disorders and is further classified into four general categories (GDA Clinical practice guidelines, 2022; ADA, 2020). All four categories fundamentally share a disturbance in the supply, as well as the action of insulin, which subsequently leads to a chronic pathologic increase in blood glucose termed as hyperglycemia (Gardner & Shoback, 2018:609). Due to their overall significant prevalence, this thesis is set to focus on the most common types of metabolic diabetes (type 1 and type 2) as well as gestational diabetes mellitus (GDM).

1.2.1.1. Type I diabetes mellitus

As described by Gardner & Shoback (2018), type 1 diabetes, as the second most common type of diabetes mellitus, is pathophysiologically attributed to the destruction and malfunction of pancreatic β-cells, ultimately leading to the state of 'absolute insulin deficiency', in which no further insulin is produced and secreted (Gardner & Shoback, 2018:609). Etiologically, in 95% of cases this is due to immune-mediated causes (type 1a), while the other 5% occur to be of idiopathic origin (type 1b).

Type 1a autoimmune reactions are caused by autoantibodies present in the blood. This includes the most frequent encountered isle cell antibodies (ICA), stimulating intracellular T-cell destruction of the pancreatic B-cells, and insulin autoantibodies (IAA), targeting circulating insulin. According to current doctrine, these autoantibodies have found to be present even years before the onset of type 1 diabetes (Gardner & Shoback, 2018:610). Basically, for type 1a and especially type 1b diabetes, a genetic cause is assumed, with association to the HLA haplotype.

1.2.1.2. Type II diabetes mellitus

In contrast to type 1 diabetes, type 2 diabetes is not initially incipient with an insulin deficiency, moreover with an insulin 'resistance', described as a decrease in tissue responsiveness to insulin (Gardner & Shoback, 2018:613). The secreted insulin itself is sufficiently present in blood circulation but it is unable to act: One of the main reasons is a malfunction in the insulin-mediated expressing of insulin-responsive glucose transporters (GLUT), whereby glucose cannot be shifted adequately into the corresponding tissue cells. It therefore remains in blood circulation and causes hyperglycemia. This ever-present

oversupply of circulating glucose steadily stimulates the pancreas to mask the insulin resistance with increased amounts of secreted insulin. At some point, however, this overproduction can no longer be maintained, causing the amount of produced insulin to drastically decrease, now present as relative insulin deficiency, and type 2 diabetes becomes manifest (Gardner & Shoback, 2018:614). Because the pancreatic depletion of B-cell function is individually varying in its extend and speed of progression, the severity of the disease can range from none or just minimal impairment in the state of incipient relative insulin deficiency, to the most severe form of absolute insulin deficiency with fatal complications, described further below (Gardner & Shoback, 2018:623). What ultimately makes type 2 diabetes so dangerous is the protracted insidious and often asymptomatic progression of the disease until it is diagnosed. In this exact time span, the profound hyperglycemia can lead to serious ostensible macro- and microvascular damage without being noticed (Gardner & Shoback, 2018:613). While the cause of type 1 diabetes is largely autoimmune-determined, type 2 diabetes is etiologically considered to be associated to a sedentary lifestyle, predominantly abdominal visceral obesity, as well as aging and putative genetic factors (Gardner & Shoback, 2018:613).

1.2.1.3. Gestational diabetes mellitus

Gestational diabetes mellitus is an occasional type of glucose intolerance that firstly develops during pregnancy. With a prevalence of 5.38% in pregnant women in 2016 in Germany, Gestational diabetes mellitus (GDM) is a rather common metabolic disorder entity (DDG & DGGG, 2018:9). According to the eminently influential ‘Hyperglycemia and Adverse Pregnancy Outcome’ HAPO study in 2008, addressing high glucose levels in pregnancy and their impact on mother and fetus, the average global prevalence of GDM occured to be 17.8%. Until today, the global prevalence of GDM has increased significantly over the last 15 years and is estimated to follow this trend in the future (DDG & DGGG, 2018:9). Pathophysiologically, an already existing pre-conceptional insulin resistance may be causal for the development of GDM, which is further exacerbated by the physiological insulin resistance occurring from 20 weeks gestation (Gardner & Shoback, 2018:678). While the first 20 weeks of pregnancy are metabolically mainly anabolic, with an increased insulin sensitivity in favor of fetal development, this anabolic state tips in the second half of pregnancy, becoming increasingly katabolic and resulting in said insulin resistance (DDG & DGGG, 2018:8). This increased, physiological insulin resistance is compensated for by an increased secretion of insulin. However, if this compensation

becomes insufficient, similar to the pathophysiological mechanisms in type 2 diabetes, GDM accompanied with hyperglycemia develops. Further, a potential mismatch in the secretion-patterns of adipokines and cytokines, starting at pregnancy week 20, is discussed, with decreased secretion of adiponectin and increased secretion of leptin and TNF-a, intermediately influencing and lowering the action of insulin (DDG & DGGG, 2018:8). In addition to potential genetic triggers, multiple risk factors have been found. These primarily include a sedentary lifestyle and obesity, like in type 2 diabetes, but also essential hypertension or pregnancy-related hypertension, a history of polycystic ovary syndrome, a history of early spontaneous abortion, as well as a history of macrosomia (Gardner & Shoback, 2018:678). In order to detect a developing GDM in time, a preventive non-fasting screening test is scheduled between gestation week 24 (24+0) and 28 (27+6) by performing a 50-g glucose challenge test (GCT). This test is regarded as positive with a venous blood glucose level of above 135mg/dl (7.5mmol/l) one hour after drinking a glucose test solution, whereby the test's sensitivity allows to identify roughly 80% of women with GDM with a result of above 140mg/dl (Gardner & Shoback, 2018:678; DDG & DGGG, 2018:19). In case the GCT turns out to be positive, a fasting 75-g-oral 2-hour glucose tolerance test (oGTT) is performed. Here, a 75g glucose solution is drunk and the venous plasma glucose concentration is determined in fasting right before the start of the test, one hour after the test and two hours after the test. If the glucose level is >92mg/dl in fasting, >180mg/dl after one hour, or >153mg/dl two hours after the test, GDM is diagnosed. On a side note, the application of the oGTT is not necessary if GCT one-hour blood glucose levels are above 200mg/dl, in this case GDM also is to be diagnosed (DDG & DGGG, 2018:32). In Austria, the application of the oGTT is included as routine testing as part of the Parents-child health passport medical examinations during pregnancy and is recommended for mothers between weeks 25 – 28 of gestation (§3 Abs. 4 S. 3 BGBl. II Nr. 470/2001 MuKiPassV i.d.F.v. 24. März 2024). Fasting blood glucose could tend to be measured as well, as it is easier and quicker to perform with higher reproducibility, and it also correlates directly with the result of the oGTT. Still, it should be considered secondary due to lack of validity as well as uncertainties regarding population-related effects. (DDG & DGGG, 2018:22). Although monitoring of diabetic adjustment in GDM using HbA_{1c} is not recommended by current guidelines, it may be initially indicative of the presence of impaired glucose tolerance as part of the screening process and it is definitely recommended to aim for a HbA_{1c} level of <7% (better <6.5%) for about 3 months before conceiving in pregestational diabetics (GDA Diabetes and Pregnancy, 2021:1; Gardner &

Shoback, 2018:679).

Regarding the clinical impact of GDM, a distinction between fetal and maternal impairments is rather useful. Acute maternal risks include an increased risk of urinary tract infections and potential associated complications. Moreover, there is an increased risk of preterm birth, as well as the development of pregnancy-induced hypertension and preeclampsia (DDG & DGGG, 2018:15). In the long term, GDM carries a huge maternal risk of developing postnatal depression, metabolic syndrome, and type 2 diabetes, with up to 60% of affected mothers developing type 2 diabetes within 10 years after birth (Noctor & Dunne, 2015). For the fetus, a major risk is the development of diabetic fetopathy including respiratory disorders as a result of disturbed surfactant formation, as well as polyglobulia and hyperbilirubinemia. In addition, the maternal hyperglycemia may result in increased stimulated fetal insulin secretion, potentially leading to serious fetal hypoglycemia. Among the long-term consequences for the child, there potentially is an early development of macrosomia, obesity, metabolic syndrome, and -as it is for the mother- a significantly higher lifetime prevalence of type 2 diabetes mellitus (DDG & DGGG, 2018:18).

Relevant to further denotation, referring to pregnancy, a previously existing type I and type II diabetes mellitus is regarded as so-called ‘pregestational diabetes’ or ‘preexisting diabetes’ (PexD), and is said to have a significantly greater maternal and fetal risk than GDM does (Sugimoto et al., 2019). According to the German Diabetes Association, in 2017, 0.93% of 761.481 pregnant women were already diagnosed with pregestational Diabetes in Germany, which 20% were considered type 2 diabetes (GDA Diabetes and Pregnancy, 2021).

1.2.2. Clinical features and effects on human microvasculature

Regarding the clinical features of diabetes mellitus, all types of uncontrolled diabetes come with a wide range of signs and symptoms. These symptoms can be acute and life-threatening such as hypoglycemia, hyperketonemia, and ketoacidosis, both mostly present in type 1 diabetes. More common symptoms are more subtle such as polyuria, due to the glucosuria, with glucose itself being osmotically and therefore diuretically active, dizziness and weakness, due to a total body potassium loss and catabolism of muscle proteins as well as paresthesia, due to the impairment of peripheral sensory nerves (Gardner & Shoback, 2018:623).

As the list of clinical symptoms continues, this thesis mainly focuses on the angiopathic

effects of diabetes mellitus related hyperglycemia. At a molecular level, there is an ongoing interaction of various pathophysiological factors related to chronic hyperglycemia. Glucose molecules itself are highly reactive, provided with 5 OH-groups. Thus, in persistent high concentrations, glucose tends to non-enzymatically glycate adjacent molecules, primarily intracellular and extracellular proteins, lipoproteins, blood cells and matrix components, as it further tends to autooxidate and lead to the production of advanced glycation end-products, known as AGEs (Rabbani & Thornalley, 2021; Gardner & Shoback, 2018:661). This glycation further leads to a malfunction, or a complete loss of function of affected molecules. If extracellular proteins and integral matrix components are affected, damage to the vascular endothelium occurs. This damage is further exacerbated by the continued local deposition of glycated, damaged proteins and blood cells which additionally corrode and thicken the basement membranes and, due to a commutation in receptor-binding, leads to activation and accumulation of macrophages causing the secretion of cytokines and interleukins, further inflaming and corroding the endothelium (Rabbani & Thornalley, 2021; Gardner & Shoback, 2018:661; Silbernagl & Lang, 2020:329). In larger vessels, hyperglycemia successively leads to atherosclerotic vascular changes through additional glycation and oxidation of low-density lipoproteins, and subsequently to peripheral arterial disease or coronary heart disease and myocardial infarction (Silbernagl & Lang, 2020:329, Gardner & Shoback, 2018:660). Regarding the microvasculature, primarily capillaries and precapillary arterioles of the renal glomeruli, as well as those of the ophthalmic retinal and choroidal vasculature, are affected by the persistent hyperglycemia and the resulting pathophysiological dysfunction, ultimately leading to diabetic nephropathy, retinopathy, or maculopathy (Gardner & Shoback, 2018:660). Indeed, the effects of long-term vascular sequelae between the types of diabetes differ. Diabetic nephropathy as well as diabetic retinopathy are usually more common in type 1 diabetes, whereas macular edema, ischemia and macrovascular damage are more common in type 2 diabetes (Gardner & Shoback, 2018:661). Nevertheless, all types of diabetes are associated with a significant risk of vascular damage and any type can be associated with any entity.

1.2.3. Diabetic retinopathy

Considering the complexity of the retinal and choroidal microvasculature as described above, it can be surmised, that such microangiopathic hyperglycemia-associated damages may eventually lead to severe impairments of ophthalmic physiological vascular

hemostasis, a clinical entity specified as diabetic retinopathy (DR). With regard to the definite pathophysiological mechanisms, an interaction of several pathogenic factors and pathways is currently being discussed (Yanoff & Duker, 2019:544; Silbernagl & Lang, 2020:328). One contributing factor may be the hyperglycemia-mediated increased concentration of aldose-reductase, present in retinal pericytes and Schwann cells. This enzyme is responsible for the metabolization of glucose into pathway-molecules, particularly sorbitol. Chronically increased levels of these osmotically active molecules lead to the swelling and dysfunction of the aforementioned cells, necessary for maintaining retina's physiological functioning and morphology. Further, a disturbance in platelet function as well as the viscosity of the blood is assumed, which subsequently leads to focal capillary occlusions and ischemia. This, accompanied by hyperglycemia-induced increased formation of fibrinogen, haptoglobin and coagulation factors V and VIII, further increases blood clotting (Silbernagl & Lang, 2020:328). Due to the glycation of hemoglobin, which ultimately reacts to HbA_{1c}, an occurring left-shift of the oxygen binding curve leads to deficiency of oxygen in the surrounding tissue, and, in combination with the previously described microangiopathy, subsequently increases hypoxia, which further results in an increased formation of hypoxia-induced factors (HIF) and subsequently in the formation vascular endothelial growth factor (VEGF), promoting regional vascular neoproliferation and abnormal retinal neovascularization (Silbernagl & Lang, 2020:328). Diabetic retinopathy is also considered to inhere a neurodegenerative component, characterized by a thinning of the INL, as well as a reduction in the number and functioning of synapses and alterations in the structure of the dendrites (Gardner & Shoback, 2018:662).

In general, DR is classified into two partly converging clinical entities (GDA Diabetic Retinopathy and Maculopathy, 2021:6; Yanoff & Duker, 2019:545). In many cases, DR tends to begin with a so-called non-proliferative type of diabetic retinopathy (NPDR). This type is strictly not accompanied by neovascularization. In the early-stage course, NPDR is characterized by the occurrence of microaneurysms (mild NPDR), which may subsequently rupture and lead to intraretinal dot hemorrhages (moderate NPDR). These, depending on their location within the retinal layering, may be difficult to detect and distinguish diagnostically (Yanoff & Duker, 2019:545). While microaneurysms tend to appear as small red dots, hemorrhages in deep layers also appear as small dots, what complicates ophthalmoscopic differentiation. In upper layers, they appear as so-called splinter shaped. Here, recent imaging such as fluorescein angiography and OCTA is being utilized, which will be further discussed in the following chapter. In advanced stages,

retinal hypoxia is exacerbated by the ongoing progression of microvascular damage. Morphologically, this is manifested by an increase in the number and size of retinal hemorrhages, whereby more than 20 microaneurysms and/or intraretinal hemorrhages in all four quadrants are considered as severe NPDR (German Medical Association, 2015:11). Furthermore, in severe NPDR, venous beading due to impaired retinal blood flow, as well as intraretinal microvascular abnormalities (IRMAs), and the appearance of cotton-wool spots, caused by vascular local ischemia and obstruction of axoplasmic flow in the NFL, resulting in swelling of nerve fiber layers, may occur (Yanoff & Duker, 2019:545). A further discussed breakdown of the inner BRB due to DR may worsen this process by leaking blood components to the neural retina (Yanoff & Duker, 2019:528). Within one year, approximately 50% of late stage NDRP tend to progress into a proliferative subtype of diabetic retinopathy (PDR) (Grehn, 2019:303). Causative for this proliferative type of DR is the increasing retinal ischemia, which, as described above, leads to gradual HIF and VEGF mediated vascular neoproliferation and retinal neovascularization. Depending on the locus of occurrence, a distinction is made between neovascularization of the disc (NVD) and neovascularization elsewhere (NVE). While NVD occurs narrowly surrounding the papilla, potentially caused by the absence of the ILM at this location, NVE tends to occur further away from the optic disc, along the retinal vascular arcs (Yanoff & Duker, 2019:546; Grehn, 2019:303). These new-formed, morphologically underdeveloped vessels originate largely from endothelial proliferations of the retinal veins and venules, as they grow through the retina towards the vitreous body and, due to their fragile, leaky vascular wall, often lead to severe vitreous hemorrhage (Grehn, 2019:303). These vessels are accompanied by a newly formed fringe of contractile fibrovascular connective tissue formations, so-called fibrovascular membranes, whose density increases with the progression of PDR. For the vitreous, this proliferation may lead to fibrous thickening and scarring of the posterior vitreous hyaloid face, which then exerts vitreous traction on the retina and can ultimately lead to traction retinal detachment and a permanent loss of vision (Yanoff & Duker, 2019:546; Grehn, 2019:303). The occurrence of neovascular glaucoma (NVG) represents a significant risk, which arises when the newly formed vessels proliferate across the anterior chamber angle as well as the iris surface, known as neovascularization of the iris (NVI), and obstruct the trabecular meshwork. In later stages, these newly formed vessels may be accompanied by fibrovascular membranes, further catalyzing the deterioration of secondary open-angle glaucoma (Yanoff & Duker, 2019:1082).

As mentioned before, all stages of DR may be accompanied by the occurrence of diabetic maculopathy. Since VEGF, as a vasopermeability factor, tends to induce leakage of free fluid into the interstitium, DR is frequently associated with diabetic macular edema (DME). In the context of NPDR, additional fluid leaks from the local microaneurysms occur, whereas in PDR, leakage is favored by the fragile neoproliferated vessels (Yanoff & Duker, 2019:544).

Although diabetic retinopathy carries a serious risk of potential blindness, the actual risk of severe visual impairment is less than 5% in case current recommendations of the Early Treatment Diabetic Retinopathy Study (ETDRS) clinical trials are followed. Thus, for example, according to the Diabetes Control and Complications Trial, a tight control of diabetes in type 1 diabetics lead to a 76% reduction in the development of DR (Grehn, 2019:301; Yanoff & Duker, 2019:543). Regarding the prevalence of DR, according to the German Diabetes Association in 2020, in Germany, 24% to 27% of type 1 diabetics and 2% to 16% of people affected by type 2 diabetes tend to have signs of retinopathy at the time of being diagnosed (GDA Diabetic Retinopathy and Maculopathy, 2021:1).

While the most apparent risk factor for developing DR is the cumulative duration of diabetes mellitus, the first five years of type 1 diabetes tend to have a fairly low risk of developing diabetic retinopathy. Although, after a time span of ten years, approximately 71-90% of people affected by diabetes have developed DR (Yanoff & Duker, 2019:543). Additional to the duration of diabetes, other risk factors, incidentally, also affecting the vasculature, such as arterial hypertension, hyperlipidemia, and smoking, also contribute to the development of DR. Important to note is a further factor, eminently promoting the development and the progression of DR, which is pregnancy, being discussed in a later chapter (Grehn, 2019:302).

In order to identify the potential presence of diabetic retinopathy at an early stage, the German Diabetes Association (2020) recommends performing ophthalmic examinations every two years in case of presence of diabetes, provided that no retinopathy or other risk factors mentioned above are present. If one or more risk factors are present, the examination interval should be shortened depending on the DR stage (GDA Diabetic Retinopathy and Maculopathy, 2021:1). Specifically in adolescents with type 1 diabetes, an ophthalmologic check-up is indicated annually. During puberty as well as during pregnancy, examinations should be performed every 3 months (Grehn, 2019:308).

Generally speaking, a physiological blood glucose concentration of HbA1c <6.5% and

physiological normotension, as well as a normolipidemic blood profile, should be maintained (Grehn, 2019:302).

1.2.4. Diabetic macular edema

The occurrence of diabetic macular edema is frequently associated with diabetic retinopathy, both in NPDR as well as PDR (Lemmen et al., 2021:457). Due to the alteration of the BRB, pathophysiologically described in detail above, especially the inner BRB, vascular leakage into the interstitial space may occur and can be further catalyzed by leakage drain from local microaneurysms as well as fragile neoproliferated vessels in (N)PDR (Yanoff & Duker, 2019:544, Neelakshi et al., 2009:4). As the inflow of fluid into the neurosensory retina exceeds the outflow, residual exudate accumulation becomes apparent. DME, as the most common cause of vision loss in patients with diabetes mellitus, is defined as a circumscribed area of retinal thickening due to the accumulation of intraretinal fluid and macromolecules, primarily in the inner and outer plexiform layers in combination with intraretinal hemorrhages and exudates at the posterior pole of the eye, usually temporal to the fovea (Bandello et al., 2017:102; Musat et a., 2015:133; Lemmen et al., 2021:457). More specifically, DME may also be classified into focal and diffuse DME, with focal DME being associated with the presence of strict localized areas of retinal thickening due to focal leakage of individual microaneurysms or clusters of microaneurysms, and diffuse macular edema being derived from extensively damaged capillaries, microaneurysms and arterioles with a broader macular thickening due to the generalized abnormal permeability of retinal capillaries (Bandello et al., 2017:104). However, in practice, this distinction is not always clear. According to current diagnostic criteria published by the ‘Early Treatment of Diabetic Retinopathy Study (EDTRS)’, a clinically significant DME is mostly present if retinal edema or hard exudates are located centrally in the macula or up to 500µm away from it, or if the intraretinal edema measures at least one papilla diameter and is located partially in an area of one optic disc diameter around the center of the macula (Lemmen et al., 2021:457, Bandello et al., 2017:102).

1.3. Imaging techniques for retinal vasculature

When it comes to diabetic eye diseases, diagnostic imaging techniques have become indispensable since decades. Regarding the imaging of the eye’s microvasculature, commonly used techniques like sonography or CT-Angiography quickly reach their limits what therefore requires the application of specially adapted imaging techniques.

1.3.1. Fluorescein angiography

Until today, Fluorescein Angiography (FA) remains the current gold standard of retinal and choroidal ophthalmologic imaging (De Carlo et al., 2015; Wright et al., 2022). By using a high-resolution fundus camera with spectral excitation and various barrier filters and further performing rapid-sequence photography of the posterior eye, FA provides the possibility of recording an intravenously injected fluorescein dye and visualizing two-dimensional image sets of retinal and choroidal vessel blood flow and architecture (Gervasio & Peck, 2022:1100; De Carlo et al., 2015).

For this purpose, a dye acting as contrast agent, so-called fluorescein sodium is used. With a peak absorption and excitation occurring at the specific wavelength range of 465nm to 490nm, fluorescein sodium tends to absorb blue light components. In fact, this spectrum is attained by superimposing a special blue exciter filter on the white light emitted by the camera (Gervasio & Peck, 2022:1100; Heimann et al., 2004:3). Now, with fluorescence occurring at a yellow-green wavelength spectrum of 520nm to 530nm, the agent reemits said light. The returning light then passes through a barrier-filter which filters out the remaining superfluous wavelengths and the dye can directly be detected. (Gervasio & Peck, 2022:1100). To further obtain the complete angiogram, repeated rapid-sequenced photographs are acquired at standardized time intervals which are then subsequently merged together. This whole process is divided into several phases: According to Gervasio & Peck (2022), the FA procedure begins with the filling of the choroidal vessels 8 to 15 seconds after intravenous injection of the sodium dye into an antecubital vein and passing through the internal carotid artery, via the ophthalmic artery into the short posterior ciliary arteries, supplying the choroid, as well as into the central retinal artery, supplying the retina, as mentioned above. Immediately afterwards, the dye begins its circulation through the retina, 9 – 18s after injection (Heimann et al., 2004:4). At this point, the sequential imaging is initiated, with a mean of one photo taken per second, to record the now beginning transient arterial phase, 1 – 2s after choroidal filling, immediately followed by the arteriovenous phase where the dye fills the retinal vessels. An early venous retinal filling is illustrated in figure 5 below. Photos are taken until peak fluorescence is reached, approximately 25 – 35s after injection. 45 to 60 seconds after the arterial phase. respectively 3 – 5 minutes after initial injection, the recirculation phase begins (Gervasio & Peck, 2022:1100; Heimann et al., 2004:4).

Abnormal or pathologic FA findings can be recognized by the detection of ‘hyperfluorescence’ as well as ‘hypofluorescence’. In terms of hyperfluorescence, different

causes can be described with the most common phenomena being the finding of leakage, which refers to the matter of fluorescein pathologically leaking the vessels and accumulating subretinally, intraretinally, or preretinally, on behalf of defects in local microvasculature. Since this particularly occurs in the context of diabetic retinopathy, which is associated with retinal neovascularization as described above, FA is a commonly relevant and indicated imaging modality for the diagnostics of DR (Gervasio & Peck, 2022:1100; De Carlo et al., 2015). In the stage of early NPDR, it can also assist in detecting patent microaneurysms, which are leaking dye (Yanoff & Duker, 2019:544). 'Pooling', on the other hand, describes the pathological gradual accumulation and presence of fluorescein in fluid-filled retinal or choroidal spaces, occurring in pathologies such as pigment epithelial detachment. On the contrary, hypofluorescence is understood to be the occurrence of 'blockage' and 'nonperfusion' in ophthalmic microvasculature (Gervasio & Peck, 2022:1101). Blockage usually results when interposing of optical density such as hemorrhage, vitreous or retinal, pigment, or fibrous tissue between the camera and the choriocapillaris is leading to an attenuated image. Nonperfusion is, as the name suggests, an impairment of corresponding vessels' perfusion, caused by vascular pathologies such as occlusions leading to retinal, choroidal, or optic nerve ischemia (Gervasio & Peck, 2022:1101). In advanced NPDR, due to the pathophysiological conditional worsening mentioned above, large areas of capillary nonperfusion can be detected by FA (Yanoff & Duker, 2019:545). In conclusion, FA has certainly proven its worth (Gervasio & Peck, 2022:1100). In the context of diabetic retinopathy, FA is helpful for determining sites of microaneurysms, determing capillary nonperfusion and confirming neovascularization. In case of diabetic macular edema, the leakage pattern in FA is helpful to differentiate diabetic macular edema from other type of macular edema (Yanoff & Duker, 2019:547). But despite all the many advantages, FA regularly reaches its limits in angiographic diagnostics and even holds some major drawbacks. First, there is the need of inducing pupil dilatation (Heimann et al., 2004:4). In addition, there is the indispensable use of a contrast agent: Although fluorescein sodium as a fluorescein dye is considered to be well tolerated and safe, nevertheless, mild adverse contrast agent-related side-effects such as transient nausea and vomiting, moderate adverse effects such as urticaria and syncope, or even severe adverse effects such as anaphylactic respiratory reactions occurred (Yanuzzi et al., 1986; Gervasio & Peck, 2022:1102). Another disadvantage is the time-consuming duration of performing the imaging process, which can take up 30 minutes (De Carlo et al., 2015). Additionally, as beneficial as the visualization of dye leaking, pooling, and staining

may be, in FA this may lead to obscuring of retinal and choroidal pathologies (De Carlo et al., 2015).

However, another incisive disadvantage of FA is the controversially discussed application of FA during pregnancy. Although this may be mainly due to its invasiveness and the lack of proper research and data clarifying its safety in pregnancy (Wright et al., 2022), still, according to Halperin & Olk (1990) the sodium fluorescein dye has been found to cross the placental barrier onto the fetus before the 15th week of pregnancy. Although the current consensus of fluorescein angiography's reasonability in performing it on pregnant patients is when 'the benefit of the procedure is likely to exceed the risks' (Medicines.org SERB, 2018; Wright et al., 2022:1.), nevertheless, caution should be exercised.

1.3.2. Optical coherence tomography

Unlike FA, optical coherence tomography (OCT) is a fully noninvasive, noncontact imaging modality that utilizes low-coherence interferometry, allowing to gather two-dimensional as well as three-dimensional cross-sectional images of the anterior eye, the optic disc, the retina, and, partly, choroidal tissue. (Yanoff & Duker, 2019:450; Grehn, 2019:54).

Technically, the OCT is based on measuring backscattered light reflections occurring at junctions of tissue layers with unequal refraction indexes, associated with an often referred to analogy to sonography, which is based on the same principle by using sound waves instead of light (Gervasio & Peck, 2022:1104). In OCT, broad-bandwidth light sources such as superluminescent diodes or femtosecond lasers, located in an OCT scanner, emit a near infrared light at ~820nm wavelength for imaging the posterior eye segments or at ~1310nm for imaging the anterior eye segments (Gervasio & Peck, 2022:1104). The light passes a splitter unit, where it is precisely split into two separate light beams moving in perpendicular arm directions: 1) a 'sample' light beam, that travels directly into the sample of interest, in this case, the posterior ophthalmic segments, as well as 2) a 'reference' light beam traveling from the splitter onto a reference mirror (Yanoff & Duker, 2019:450). After reaching the mirror, respectively, penetrating the scattering tissue medium, both light beams are directly getting backscattered until they recombine. If the difference in optical path length (OPL) between the interferometer's two arms, and therefore the previous covered distance of the light beams, is less than the light's coherence length, respectively, measurably nearly the same length, interference fringes can be observed, which are then detected by an OCT detector (Yanoff & Duker, 2019:450). Every time interference is

detected, it is to be concluded, that both light rays must have traveled that distinct, same way. The fixed, known reference beam's distance, reaching from the splitter up to the mirror and back, can directly be measured, and the sample beam's covered distance can therefore be determined indirectly, indicating the axial depth of a precise point of the sample tissue. Thus, it becomes possible to record a complete depth profile of the sample reflectivity at the beam position, known as A-Scan. (Aumann et al., 2019:61; Yanoff & Duker, 2019:450). In further consequence, by scanning the sample beam laterally across the sample, OCT allows to obtain a so-called cross-sectional tomogram (B-Scan). This kind of OCT is realized as Time-Domain OCT (Aumann et al., 2019:61). Based on these principles, a plethora of further constantly improving OCT techniques have been introduced over the years, particularly varying in resolution, application time and functionality.

In addition to the exceptional capability of producing high resolution images of the retinal, choroidal, and optic disc morphology as well as cross-sectional imagines of retinal architecture, these advantages justify OCT's nowadays indispensable use in diagnosis and description of preretinal, intraretinal and subretinal abnormalities and pathologies (Yanoff & Duker, 2019:452). Preretinal abnormalities may include macular holes, lamellar holes, as well as vitreomacular traction and posterior vitreous detachment, for which OCT imaging is the current gold standard. As for severe stages of diabetic retinopathy, the detection of fibrous thickening and scarring of the posterior vitreous hyaloid face, is ensured by OCT. Among the intraretinal pathologies, macular edema is the most prominent pathology to be assessed by OCT (Yanoff & Duker, 2019:452/547). Subretinal abnormalities include pathologies such as subretinal fluid, which OCT depicts as an empty space between retina and underlying retinal pigment epithelia (Yanoff & Duker, 2019:453).

1.3.3. Optical coherence tomography angiography

As the name suggests, OCTA is a novel enhanced ophthalmologic imaging modality, extending the technical principles of OCT. After the initial clinical approval of the OCTA by the U.S. Food and Drug Administration in 2016, the diversely applicable device has opened itself up for more and more imaging scenarios and indications over the past years (Yanoff & Duker, 2019:457; De Carlo et al., 2015).

Technically, OCTA takes advantage in detecting temporal changes in the reflective, light scattering behavior of the retina and the choroid by displaying constantly moving particles,

primarily erythrocytes, circulating the vessels, in contrast to the static surrounding retinal and choroidal tissue, which, in further consequence, allows generating a volumetric angiographic three-dimensional representation of the posterior ophthalmic microvasculature (De Carlo et al., 2015; Yanoff & Duker, 2019:457). This makes the OCTA a rather suitable imaging tool for examining and evaluating retinal vascular diseases. Functionally, the OCTA-device records multiple, commonly five to fifteen OCT B-Scans performed from the exact location and computes them together to detect and localize distinct changes in backscattered signal strength, known as decorrelation (De Carlo et al., 2015). Practically, this is achieved by comparing and contrasting the signal strength of each single pixel between the successively taken images and displaying those exact pixels showing a shift in signal intensity. This change in signal intensity is now deducing particle movement in light marked areas, which can be interpreted as the presence of vasculature through which the red blood cells circulate (BVA, 2017:2). To provide quantitative analysis about vessel density, the proportion of blood flow, measured at pixels with signal changes, is set in relation to the total retinochoroidal area recorded (Lang et al., 2016:2). In addition, modern OCTA-devices provide the possibility of displaying corresponding OCT B-Scans in parallel to the OCT angiograms. This enables locating structural data cross-sectionally (De Carlo et al., 2015): Thus, OCTA ultimately offers provision of both, morphological information and, superficially, functional perfusion information (De Carlo et al., 2015; BVA, 2017).

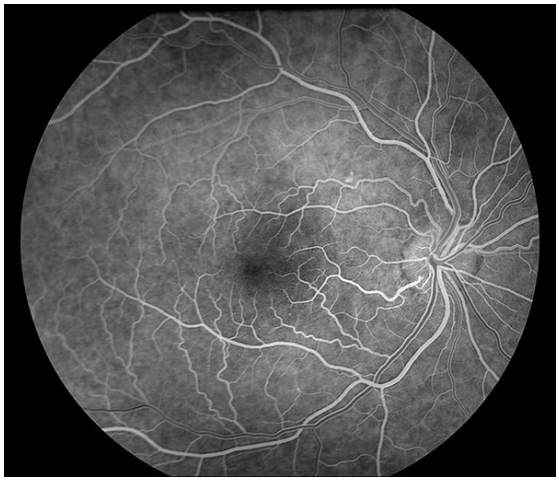

Figure 5. Imaging characteristics of fluorescein angiography. Early venous phase of the right eye, showing the retinal arcs as well as the vessel-free macula. (Reprinted from UIHC Department of Ophthalmology, 2022)

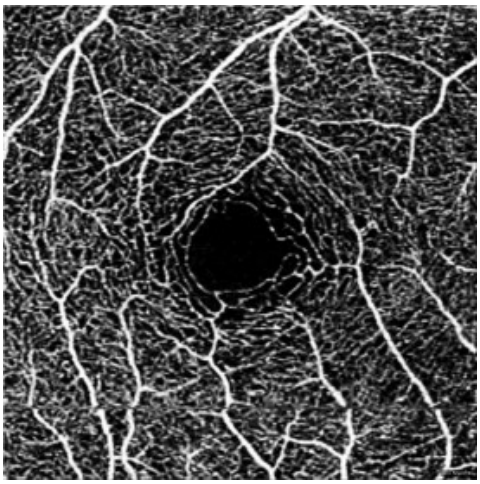

Figure 6. Imaging characteristics of OCTA. OCTA of the right eye, detailed multilayered view of the microvasculature including vessel-free FAZ.
(Reprinted from O'Keefe, Ghazala D., 2022)

Current OCTA devices are able detect blood flow with a mean perfusion rate between 0.3 – 3.3mm/s, while flow rates outside this range appear as so-called "nonperfusion" (Yanoff & Duker, 2019:457). Unfortunately, nonperfusion elucidates the trend of pathologies like microaneurysms not being detected as frequently on OCTA as on FA in general. Especially sclerosed or clotted microaneurysms without active blood flow will not appear at all (Yanoff & Duker, 2019:457-458). In a comparative context, it is necessary to highlight that OCTA, which is based on light scattering from red blood cells, in contrast to FA, cannot display dye diffusion, indicating pathologies linked to fluid leakage and blood-barrier malfunctions, as leakage remains undetected in OCTA (Lang et al., 2016:4; De Carlo et al., 2015; Yanoff & Duker, 2019:457). In addition, the omission of using an externally supplied contrast agent also brings a major disadvantage: Since OCTA utilizes the motion of circulating red blood cells, similar dense and sized particles such as lipid particulates may interfere and lead to artefactual signals (Yanoff & Duker, 2019:457).
Regarding current clinical and scientific usability, the distinguished combination of SD-OCT scans and OCTA angiograms provides a variety of applications ranging from the monitoring of regions of impaired perfusion by relying on the previously discussed condition of 'nonperfusion', to the detection of choroidal neovascularization, in pathologies such as age-related macular degeneration, to the quantification of vascular changes in retinal vascular diseases, such as diabetic retinopathy. (Yanoff & Duker, 2019:460, Grehn, 2019:339). Although OCTA is capable of imaging choroidal

microvasculature, due to the increased signal opacity of the RPE it is less accurate than dye-based angiography with regard to the detection of choroidal neovascularization (Yanoff & Duker, 2019:458-460). Regarding the retinal microvasculature, according to Spaide et al. (2015, as cited in Yanoff & Duker, 2019), OCTA has shown to superiorly visualize the radial peripapillary and deep capillary networks in contrast to FA. Due to the absence of potentially obscuring dye leakage combined with the computational segmentation and an eminent depth resolving capability, the lesion's exact axial location as well as size delineation can be adequately examined by OCTA (De Carlo et al., 2015:2). Furthermore, OCTA is an excellent tool for quantifying and monitoring subtle changes in retinal and choroidal microvasculature. According to current literature, this potential is vital when it comes to the investigation of diabetic retinopathy, in which the capillary density, measured by OCTA, significantly correlates with the clinical severity (Kim et al., 2016; Yanoff & Duker, 2019:460). Still, it remains to be mentioned that, according to the Bundesverband der Augenärzte Deutschland (BVA), a functional diagnostic assessment solely based on the OCTA is yet not recommended (Löwen, J., 2017).

Due to the utilization of red blood cells as an endogenous contrast agent, unlike in FA, noninvasive visualization of the microvasculature is achieved without the need of invasively administering a fluorescein dye. Additionally, because each three-dimensional OCTA scan-set takes up to approximately six seconds to obtain, and therefore having a fairly short acquisition time, OCTA is seen to be more practical in use for fast posterior ophthalmic imaging in several contexts (De Carlo et al., 2015). OCTA also provides the opportunity of performing scans without precipitating pupil dilatation. Although sufficient fundus illumination must be ensured, OCTA warrants ophthalmologic imaging in physiological miosis (Chanwimol et al., 2019; Löwen, J., 2017). While FA is insufficiently accommodating in dealing with mismeasurements due to its invasiveness and duration of acquisition, individual OCTA measurements can be repeated as often and as frequent as desired (Yanoff & Duker, 2019:459). Furthermore, while FA is only capable of visualizing 40% of retinal capillaries outside the foveal center and is further unable to resolve the radial peripapillary capillary plexus and the capillaries in deep retinal layers, OCTA proves to be significantly more precise and manages to resolve retinal microvasculature in detail approaching actual histology's resolution (Yanoff & Duker, 2019:458-459). In addition, given all of said advantages, OCTA is suitable for use in pregnancy without hesitation (De Carlo et al., 2015).

As mentioned above, for its precise microvasculature functional analysis, OCT-angiograms

are subsequently further anatomically segmented. Although, this segmentation is done automatically by OCTA-devices, different devices might perform differing segmentation and thus values may not always be comparable, therefore segmentation should priorly be specified in dependence of the used apparatus and OCTA device in each case (Lang et al., 2016; De Carlo et al., 2015; BVA, 2017:3). As already illustrated in figure 3, the segmentation itself allows a more subtle visualization of the neural retina, which extends into the superficial capillary plexus (SCP) and deep capillary plexus (DCP) described in chapter 1.1.3. (Lang et al., 2016).

To ensure such detailed angiographic examination, a variation in image resolution may assist. By using higher resolution in the range of 5.7 µm/px on 3x3mm in area, visualization of small capillaries is ensured, while a coarse resolution on a picture detail level of 12x12mm may aid in visualizing greater areas (BVA, 2017:3). As this high-resolution but small field of view image was one of OCTA's biggest drawbacks, the use of wide-field OCTAs, with a field of view of up to 80◦ of the fundus, is becoming more and more common. (Wright et al., 2022:2).

1.4. Pregnancy, diabetes and their impact on the eye's vascular system

While the impact of diabetes mellitus on the vasculature of the posterior eye, as discussed in the previous chapters, is uncontested, occasionally, metabolic changes and their impact on the vasculature have received more attention in recent times. Pregnancy, in fact, also represents a period of significant metabolic processes, as it alters the ophthalmic microvasculature and is strongly interdependent with present diabetes mellitus.

Pregnancy involves physiological changes in several ways, such as adaptions in the endocrine, cardiac, renal, hematologic and vascular system, and most of these processes are said to be fully reversed after delivery (Ouzounian & Elkayam, 2012 cited in Chanwimol et al., 2019). Regarding the vascular system, an increase in plasma volume of about 50% occurs between gestational weeks 6 and 32, while at the same time, arterial under-filling occurs, as almost 85% of the blood volume remains in the venous circulation. In addition, peripheral vasodilation occurs with a concomitant decrease in systemic vascular resistance. This decrease in vascular resistance also occurs in the ophthalmic vascular system, as elevated levels of estrogen lead to vasodilation. In addition, an increase in ocular blood flow was demonstrated (Kızıltunç et al., 2020), combined with an increase in hydrostatic capillary pressure (Chanwimol et al., 2019:3).

In terms of diabetes mellitus, there is strong evidence that pregnancy facilitates the

progression of diabetic retinopathy (Grehn, 2019:303; Sugimoto et al., 2019:4). In addition to the increased retinal blood flow, this could be explained by an upregulation of circulating IGF-1 and C-reactive peptide (Sugimoto et al., 2019:4). Furthermore, previous studies have shown that in diabetic eyes, vascular malformations such as microaneurysms may already exist even without the presence of diabetic retinopathy. Otherwise, the risk of developing NPDR is estimated to be 10% for pregnant diabetic women without diabetic retinopathy. However, post-partum, there is said to be some regression regarding DR (Yanoff & Duker, 2019:543; Gardner & Shoback, 2018:675). Concerning the eyes, GDM is held responsible for the occurrence of retinal vascular changes like narrower vessel caliber, larger vessel branching and reduced vasodilatory response (Liu & Wang, 2021).

1.5. Current literature: Insights and discrepancies

As OCTA has already proven itself as a successful ophthalmic imaging alternative in detecting and monitoring diabetic retinopathy in pregnant patients in comparison to invasive FA (Wright et al., 2022), with the use of OCTA, the number of studies examining the impact of pregnancy on the ophthalmic microvasculature grew significantly over the past few years. However, the results are still conflicting.

In this context, a study conducted by Hepokur et. al. published in 2021 was able to confirm the assumption, that retinal vasculature was indeed affected by physiological changes during pregnancy. The researchers were able to show that in the parafoveal retinal region, the vessel density of the SCP in pregnant women was significantly lower than in non-pregnant women, while other retinal zones did not significantly differ in vessel density of SCP. In general, no changes in vessel density were observed for DCP or RPCP. Regarding the size of the FAZ, no difference in size was observed for pregnancy in general and within pregnancy between the three trimesters.

Kızıltunç et al. (2020) were also able to conclude that retinal, choroid, and optic disc microvasculature was affected by physiological changes during pregnancy. More precisely, they found out, that the vessel density of SCP in whole macula, perifoveal retina, as well as the parafoveal retina, was significantly higher in pregnant women than it was in non-pregnant women. At the same, foveal vessel density in the SCP was significantly lower in pregnant women compared to non-pregnant women, directly linked to an increase in FAZ size in pregnant women. In DCP, vessel density regarding the whole macula as well as the perifovea area was higher in pregnant women than it was in non-pregnant women. The foveal and parafoveal vessel density of the DCP did not differ between pregnant and non-

pregnant women. As in the study by Hepokur et al. (2021), vessel density of SCP, DCP and RPCP did not differ between the three trimesters. It is important to note that the comparisons between the different trimesters in both studies were not based longitudinally on changes within the same individuals over time, but the participants were enrolled into three groups according to their trimester.

Another study conducted by Chanwimol et al. (2019), investigating the effects of pregnancy on retinal microvasculature, showed a lower perfusion density of the SCP in pregnant women than in non-pregnant women, regarding the whole macula, contrary to the results of the abovementioned study by Kızıltunç et al. (2020). Additionally, perfusion density within the pregnant women was higher in the parafovea area than it was within the non-pregnant women. Here, too, the size of the FAZ did not differ in size between pregnant women and non-pregnant women.

In order to investigate a potential effect of diabetes mellitus on retinal microvasculature in pregnant women, Sugimoto et al. (2019) conducted a study in which they included women with preexisting diabetes as well as gestational diabetes mellitus and used the FAZ as an inverse morphological indicator for perifoveal microcirculation and vascular density. If put in the context of the studies already cited, no inherently mediated influence of diabetes mellitus on the microvasculature was determined, as the size of FAZ of the SCP, as well as DCP, did not differ between PexD, GDM and healthy pregnant women at any time during pregnancy. However, there was a significant negative correlation between SCP-FAZ and number of weeks of pregnancy, indicating a decrease in FAZ size, possibly associated with an increase in (peri-)foveal vessel density of the SCP, over the course of pregnancy.

To assess the influence of gestational diabetes on retinal microvasculature more accurately, Liu & Wang, (2021) conducted yet a similar OCTA study. According to their research, pregnant women, and women with GDM had a lower SCP vessel density in whole macula, foveal, and parafoveal compared to non-pregnant women, although said vessel density did not differ between pregnant women and pregnant women with GDM. However, regarding the DCP, pregnant women with and without GDM showed a larger vessel density in whole macula and the parafoveal area compared to non-pregnant women, with, again, no difference in vessel density between pregnancy and GDM. The foveal vessel density of the DCP, on the other hand, was smaller in pregnant women with and without GDM, like it was in SCP. In addition, pregnant women showed a larger FAZ compared to non-pregnant women, while there were no differences in FAZ size between pregnant women and women with GDM.

Consistent within the studies of Chanwimol et al. (2019) and Liu & Wang (2021) is a lower SCP vessel density in whole macula in pregnant women, while vessel density of DCP was higher, particularly in parafoveal areas. Moreover, as in the study by Sugimoto et al. (2019), no difference was found in terms of FAZ size between pregnant women and women with GDM. As Chanwimol et al. (2019) hypothesized a potentially different influence pattern on the vessels of the SCP as opposed to those of the DCP due to differences in hydrostatic pressure, structure, and function, Liu & Wang (2021) further examined plexus capillary morphology. They discovered relatively loosened vascular branches in the SCP in pregnant women, but dense vascular branches in the DCP. According to Coscas et al. (2016), one further explanation for the increasing effects on DCP vessel density in contrast to SCP, in the context of high hydrostatic pressure, may be a mediating interconnection of transverse venules between DCP and superficial major veins, which has already been found in mice. Yet, in general, the study by Kızıltunç et al. (2020) showed conflicting results. Liu & Wang (2021) concluded that also different inspection equipment and variable imaging quality may have led to such differing results.

1.6. Study aims, rationale and hypotheses

This study aims to provide further evidence on the effects of pregnancy, preexisting diabetes, and gestational diabetes on vessel density of SCP, DCP, RPCP, as well as the FAZ and to further assess these potential effects across multiple time points during pregnancy with the help of OCTA.

In accordance with the results obtained by Chanwimol et al. (2019) and Liu & Wang (2021), lower percentages in vessel density of the SCP and, in parallel, higher vessel density of DCP is to be assumed in pregnant women with and without diabetes mellitus in contrast to non-pregnant women. Since diabetes mellitus had no effect on vessel density of neither SCP, nor DCP in pregnant women, this is also assumed to be the case for this study. No difference in vessel density of SCP or DCP, as well as no difference in FAZ size is to be assumed between pregnant women and pregnant women with diabetes at a single time of survey. Regarding the FAZ, no differences in size are to be expected between pregnant women with and without diabetes mellitus and non-pregnant women at any given time in pregnancy.

2. Material and Methods

2.1. Sample, patient recruitment, inclusion criteria, exclusion criteria

The study sample included a total of 39 women, enrolled into four study groups. The first group included 3 healthy pregnant women without diabetes mellitus. The second group included 12 women with preexisting diabetes mellitus type 1 and type 2 (PexD), while the third group included 5 women with gestational diabetes mellitus (GDM). The fourth group, serving as a control group, consisted of 19 age-matched healthy non-pregnant women without any type of diabetes mellitus. This study was conducted in full conformity with the 1964 Declaration of Helsinki and all subsequent revisions.

The recruitment of patients was carried out by the Division of Endocrinology and Diabetology of the Department of Internal Medicine, by the Department of Obstetrics and Gynecology, and by the Department of Ophthalmology of the Medical University of Graz. Included were women with an age ranging between 25 and 40 years, given an informed consent in written form. Time of inclusion for the pregnant women was required to be between the 25^{th} – 28^{th} week of pregnancy, after the oGTT was performed. Specifically, the pregnant women without diabetes mellitus (group 1) should exhibit an one hour-plasma glucose level of less than 140mg/dl in oGTT, while the pregnant women with diabetes mellitus (group 2 and group 3) had to exhibit a HbA_{1C} value of less than 10% or 85.8mmol/mol at the time of examination. For the healthy non-pregnant women (group 4), the fasting plasma glucose had not to exceed an abnormal value of >7.0mmol/l or 126mg/dl after a fasting period of 8 – 12 hours (GDA Clinical practice guidelines, 2022). Additionally, uncontrolled hypertension, multiple pregnancy, refractive errors of more than 6 diopters in spherical equivalent, calculated by disregarding the axis and adding half the cylinder power to the sphere power, or any condition possibly interfering with trial participation or evaluation of results, as judged by the investigator, lead to exclusion (Yanoff & Duker, 2019:41).

2.2. Patient examinations

Regarding the visit schedule, to warrant a repeated measures design, two time points of evaluation were defined. The baseline visit was conducted at the onset of the study between weeks 25 – 28 of gestation. The follow-up visit took place at weeks 37 – 40 of gestation. At baseline, in addition to obtaining the informed consent and verifying inclusion and exclusion criteria, further demographic data, past medical history, data on current medication intake, and history of tobacco and alcohol intake was obtained. While

HbA_{1c} testing was performed for the pregnant women, plasma glucose levels were determined from fasting blood glucose for the control group (group 4). Additionally, current weight and height for further determining the body mass index was assessed. Subsequently, without dilation, OCTA, as well as OCT, were performed, with more detailed specifications described further below. In addition, autorefraction was performed to calculate the spherical equivalent and fundus photography to identify potential interfering conditions that would result in exclusion. As part of the follow-up visit, glucose testing, OCTA, OCT, autorefractometry, and fundus photography were performed a second time. A concise overview is shown in table 1.

Table 1

Study schedule including performed testing and imaging for the pregnant and non-pregnant women each at baseline and follow-up visits.

	Baseline Visit (weeks 25-28 of gestation)	Follow-Up Visit (weeks 37-40 of gestation)
Informed consent	X	
Medical history, demographic data, height, weight	X	
HbA1c testing and blood glucose testing	X	X
OCTA	X	X
Fundus photography	X	X
OCT	X	X
Autorefractometry	X	X

2.3. Ophthalmological examination and image acquisition

For the acquisition of OCTA scans, the AngioVue^{TM} spectral-domain OCT (SD-OCT) Imaging System (RTVue XR Avanti, Optovue INC., Fremont, CA, USA), utilizing a split-spectrum amplitude decorrelation algorithm in software version 2018.1.1.69, was applied.

Along with its capability of capturing 70.000 A-Scans per second via an 840nm light source, including all common scan sizes varying from 3 x 3mm to 6 x 6mm to 8 x 8mm for retina and 3 x 3mm to 4.5 x 4.5mm for optic disc, it further provides the option of capturing 12 x 8mm widefield (40°) images of the retina (De Carlo et al., 2015:4; Eyefox, 2023). Segmentation into the respective vessel plexus is performed automatically. As already mentioned above, the SCP as measured by OCTA consists of the projection of the vessels within the RNFL, the GCL and parts of the IPL. The DCP is located in between the IPL and the OPL (Hepokur et al., 2021:2; Ki-Yup et al., 2022:3, Campbell et al., 2017:1). In addition, the device also segments an outer retinal area as well as the choriocapillaris, resulting in a total of four segments (De Carlo et al., 2015:4; Eyefox, 2023). Images used for evaluation had to possess a signal strength index of over 70, and a quality index greater than 5. A scan size of 6 x 6mm was utilized for imaging the retina, whereas the disc was recorded within a 4.5 x 4.5mm scan size. Regarding the macular and optic disc regions, three areas were set. With a diameter of 1mm the foveal zone was located centrally. Surrounding it was the parafoveal zone with a diameter of 3mm excluding the central foveal zone. The outermost zone with a diameter of 6mm defined the perifoveal zone, excluding the foveal and the parafoveal zone (Kızıltunç et al., 2020:3). The retinal mapping is further illustrated in figure 7. The optic disc was divided into two sections. Centrally located was the 2mm wide inside disc. Surrounding this area was the peripapillary region, up to a diameter of 4mm excluding the inside disc. While the segmentation of SCP and DCP has already been described above, vessel density was operationalized as the percentage of vasculature with active blood flow in proportion to the total respective area assessed (Kızıltunç et al., 2020:2). As part of the peripapillary assessment, the thickness of the RNFL as well as the vessel density of RPCP was analyzed. The central retinal thickness (in μm) was determined automatically by the RTVue XR software and was measured foveal reaching from ILM to RPE. The size of FAZ (in mm^2) as well was determined automatically.

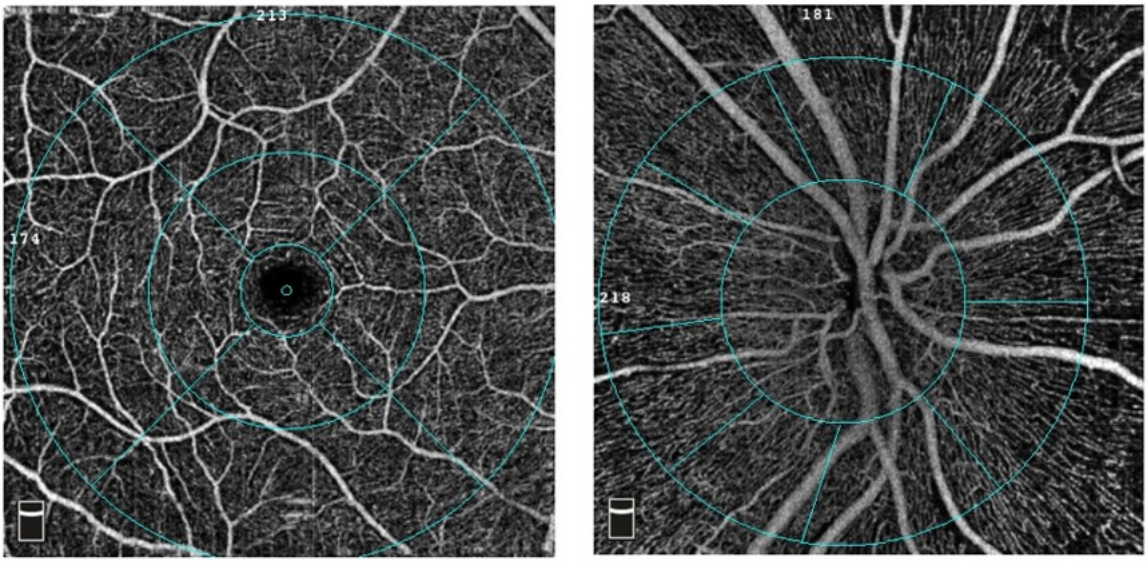

Figure 7. Subdivision of macula and optic disc in further areas by OCTA.
(Left). Subdivision of macula with the centrally located foveal zone (d=1mm) surrounded by the parafoveal zone (up to d=3mm) as well as the perifoveal zone (up to d=6mm). *(Right)*. Subdivision of the optic disc with the centrally located inside disc zone (d=2mm) surrounded by the peripapillary zone (up to d=4mm).
(Own illustration captured in RTVue XR Avanti, 2023)

For acquiring OCT cross-sectional images, the Spectralis spectral-domain (SD) optical coherence tomography device (Heidelberg Engineering, Inc., Heidelberg, Germany) was applied. To avoid artifacts such as light scattering and absorption, and to further increase the level of detail in choroid, enhanced depth imaging (EDI) was utilized, wherefore the OCT device is moved closer to the eye for shifting the peak sensitivity curve closer to the choroid in SD-OCT and further averaging nearly 100 images together for improving image resolution. (Yanoff & Duker, 2020:455). Additionally, subfoveal choroidal thickness was assessed by manually measuring and quantifying the whole choroid across its entire foveal width in the foveal region SD-OCT in SD-OCT images.

2.4. Study design, variables and statistical analyses

The study was designed as a prospective cross-sectional, single-centered study. A previously performed sample size estimation with an estimated statistical power of 0.8 and a 5% type-I-error recommended a total sample size of 64 women, including 16 women in each of the 4 groups. Since the current thesis, as a preliminary evaluation, certainly is restricted in time and resources, an inferential statistical analysis is only performed in the case of a respective subsample size of $n = 16$ participants for each group, otherwise, a descriptive data evaluation is performed, which involves calculating and reporting the mean of differences for the individual values in dependent variables outlined further below

between both visits. In statistical terms, the study is conducted as a repeated-measures experimental 4 x 2 design with the the group-assignment for groups 1 – 4 as the between-subjects factor. The within-subjects factor involved the assessment of the dependent variables across the two times of examination, further indicating the weeks of gestation. Thus, the assignment to the four groups simultaneously represents the independent variable. The foveal retinal thickness, the RNFL thickness, the whole macular as well as the foveal vessel density of SCP and DCP, the vessel density of RPCP, and the size of the FAZ, all measured using OCTA, as well as the choroidal thickness, measured using OCT, represent the dependent variables. The dependent variables were analyzed for each participant across both eyes in total, providing that only valid complete pairs of data for both eyes across both visits were available. Parafoveal and perifoveal retinal sections as part of vessel density analysis were not evaluated. Statistical analysis was performed using SPSS Statistics for Windows version 29 (IBM Corp., Chicago, IL, USA).

3. Results

3.1. Demographics

At the end of the investigation period and data collection applicable for the current thesis, a total of 39 women with a total of 78 eyes and a mean age of 32.6 years (*SD* 4.6) participated in the study. Examining the four individual study groups, the 3 healthy pregnant women had a mean age of 32.3 years (*SD* 1.6). Their mean spherical equivalent was -0.2 D on the right eye (*SD* 0.2) and -0.6 D on the left eye (*SD* 0.1). The mean body mass index was 27.0 kg/m^2 (*SD* 2.0) at the time of examination in 25 – 28 weeks of pregnancy and 24.0 kg/m^2 (*SD* 1.0) before the start of pregnancy. The second group, including 12 pregnant women with preexisting diabetes mellitus type 1 and type 2, had a mean age of 33.2 years (*SD* 4.0). The mean spherical equivalent in this group was -1.2 D on the right eye (*SD* 1.0) and -1.3 D on the left eye (*SD* 1.0). While their mean body mass index was 25.6 kg/m^2 (*SD* 2.5) at the time of the examination, it was 22.3 kg/m^2 (*SD* 2.1) before the start of pregnancy. The 5 pregnant women with gestational diabetes mellitus had a mean age of 34.8 years (*SD* 5.8). Their mean spherical equivalent was -1.3 D on the right eye (*SD 1.0*) and -1.4 D on the left eye (*SD* 1.0) while their mean body mass index was 31.6 kg/m^2 at the time of examination (*SD* 2.1) and 29.1 kg/m^2 before the start of pregnancy (*SD* 3.7). The 19 healthy non-pregnant women had a mean age of 31.7 years (*SD* 5.0). The spherical equivalent was -2.0 D on the right eye (*SD* 2.0) and -1.7 D on the left eye (*SD* 2.0). The mean body mass index was 22.7 kg/m^2 (*SD* 4.5) at the time of examination. Regarding the blood glucose levels, the healthy pregnant women showed a mean fasting blood glucose of 68mg/dl (*SD* 1.0), whereby none of the individual participants had pathologically elevated blood glucose levels exceeding 126mg/dl at the time of examination. For the pregnant women with diabetes mellitus, the mean HbA_{1C} was 38.7 mmol/mol (*SD* 7.0) in the women with preexisting diabetes mellitus and 34.5 mmol/mol (*SD* 4.0) in the women with gestational diabetes mellitus. Since all participating pregnant women with diabetes mellitus were adequately controlled by medication and therefore no HbA_{1C} values of more than 86.8mmol/mol were present, no participants were excluded. Within the healthy non-pregnant women, the mean fasting blood glucose was 91mg/dl (*SD* 8.0). Again, none of the participants was excluded. A concise summary of respective demographics is found in table 2 below.

Table 2

Demographic data including age, spherical equivalent (SE) of each eye, body mass index (BMI) and blood glucose levels for all four study groups.

	Mean			
Parameters	**Healthy Pregnant (*n* = 3)**	**PexD (*n* = 12)**	**GDM (*n* = 5)**	**Healthy non-pregnant (*n* = 19)**
Age	32.3 (1.6)	33.2 (4.0)	34.8 (5.8)	31.7 (5.0)
SE Right Eye (in diopters)	-0.2 (0.2)	-1.2 (1.0)	-1.3 (1.0)	-2.0 (2.0)
SE Left Eye (in diopters)	-0.6 (0.1)	-1.3 (1.0)	-1.4 (1.0)	-1.7 (2.0)
BMI week 25–28 (in kg/m²)	27 (2.0)	25.6 (2.46)	31.6 (2.13)	22.7 (4.5)
BMI before pregnancy (in kg/m²)	24 (1.0)	22.31 (2.1)	29.1 (3.65)	/
Fasting Blood Glucose (in mg/dl)	68 (1.0)	/	/	91 (8.0)
HbA_{1C} (in mmol/mol)	/	38.7 (7.0)	34.5 (4.0)	/

During the review of fundus photography, none of the participants was found to have any pathological susceptibility that would have led to exclusion.

3.2. Results of ophthalmological examination

The following section outlines and describes the results of imaging and quantification of retinal as well as choroidal vasculature, with specific examination of retinal-, choroidal-, and RNFL thickness, of vessel density of SCP, DCP and RPCP, as well as of FAZ size. As, at the time of data analysis, an adequate number of participants in the group of healthy pregnant women was yet not sufficiently achieved, and none of the women with gestational diabetes mellitus had yet attended the follow-up examination for the present thesis, predetermined prerequisites for an inferential statistical multivariate analysis of data were violated. Therefore, a preliminary descriptive evaluation of data collected so far, serving as an interim analysis, is performed and recorded, considering both eyes collectively. Certain limitations in data collection, statistical evaluation and general interpretation of data are further outlined in the discussion below.

3.2.1. Retinal thickness

Within the healthy pregnant women, the mean foveal retinal thickness was 259µm (*SD* 8) at weeks 25 – 28 of gestation. At weeks 37 – 40 of gestation it was 257µm (*SD* 8). In descriptive terms, based on the mean of differences outlined above, a mean decrease of -2.00µm (*SD* 0.82) could therefore be determined. Regarding the pregnant women with preexisting diabetes mellitus, at the time of the baseline examination, a mean retinal thickness of 257µm (*SD* 15) was observed. At the time of follow-up, the mean retinal thickness was 258µm (*SD* 15), corresponding to a mean descriptive increase of 1.00µm (*SD* 2.00) in central retinal thickness. Within the pregnant women with gestational diabetes mellitus, a mean retinal thickness of 255µm (*SD* 18) was observed. However, as none of the respective participants had yet completed the corresponding follow-up examination at 37 – 40 weeks of gestation at the time of data evaluation, currently no further information on the absolute and relative changes in retinal thickness between both times of examination may be provided. The healthy non-pregnant women had a mean retinal thickness of 256µm (*SD* 15) at the time of the baseline examination as well as a mean retinal thickness of 255µm (*SD* 16) at the time of follow-up. Descriptively, these data suggest a mean descriptive decrease of -1.26µm (*SD* 1.94) in retinal thickness. Respective descriptive data are shown in table 3.

Table 3

Mean retinal thickness across all study groups considering both eyes collectively at baseline and follow-up visit as well as corresponding standard deviations. The change in vessel density was calculated by using the mean of differences.

	Mean			
	Healthy Pregnant (*n* = 4)	**PexD (*n* = 11)**	**GDM (*n* = 8)**	**Healthy non-pregnant (*n* = 38)**
Baseline retinal thickness (in µm)	259 (8)	257 (15)	255 (18)	256 (15)
Follow-up retinal thickness (in µm)	257 (8)	258 (15)	/	255 (16)
Change in retinal thickness (in µm)	-2.00 (0.82)	1.00 (2.00)	/	-1.26 (1.94)

3.2.2. Choroidal thickness

In terms of choroidal thickness, a mean increase of 53.00µm (*SD* 1.41) was descriptively observed within the healthy pregnant women. At the time of the baseline visit at weeks 25 – 28 of gestation, the mean choroidal thickness was 439µm (*SD* 9), while at the time of follow-up at weeks 37 – 40 of gestation, it was 492µm (*SD* 8). Within the pregnant women with preexisting diabetes mellitus, a mean choroidal thickness of 347µm (*SD* 98) was measured at the time of the baseline visit, while it was 308µm (*SD* 78) at the time of follow-up. Thus, a mean descriptive decrease of -38.89µm (*SD* 24.54) was observed. In the pregnant women with gestational diabetes mellitus, the mean choroidal thickness was 271µm (*SD* 54) at the time of the baseline visit. Since, as previously mentioned, at the time of data evaluation there yet was no second point of examination within the pregnant women with GDM, no change in choroidal thickness could be reported. The mean choroidal thickness within the healthy non-pregnant women was 317µm (*SD* 84) at weeks 25 – 28 of gestation and 318µm (*SD* 90) at weeks 37 – 40 of gestation. With an observed mean increase of 0.65µm (*SD* 16.38), there was descriptively almost no change in choroidal thickness between the two times of evaluation, as it was observed with retinal thickness. For illustration, the descriptive data regarding the choroidal thickness are shown in table 4.

Table 4

Mean choroidal thickness across all study groups considering both eyes collectively at baseline and follow-up visit as well as corresponding standard deviations. The change in vessel density was calculated by using the mean of differences.

	Mean			
	Healthy Pregnant (*n* = 2)	**PexD (*n* = 9)**	**GDM (*n* = 8)**	**Healthy non-pregnant (*n* = 34)**
Baseline choroidal thickness (in µm)	439 (9)	347 (98)	271 (54)	317 (84)
Follow-up choroidal thickness (in µm)	492 (8)	308 (78)	/	318 (90)
Change in choroidal thickness (in µm)	53.00 (1.41)	-38.89 (24.54)	/	0.65 (16.38)

3.2.3. Retinal Nerve Fiber Layer (RNFL) thickness

The evaluation of the RNFL thickness, measured peripapillary, surrounding the optic disc region, showed a mean thickness of 102µm (*SD* 1) in healthy pregnant women at the time of the baseline examination. At follow-up, the mean RNFL thickness was 100µm (*SD* 6). Calculated on the mean of differences, this descriptively equals a mean decrease of -1.50µm (*SD* 4.95). In the pregnant women with preexistent diabetes mellitus, the mean RNFL thickness at baseline was 109µm (*SD* 11). At the time of follow-up, they showed a mean thickness of 110µm (*SD* 14). This results in a mean descriptive increase in RNFL thickness of 0.67µm (*SD* 3.06). Within the pregnant women with gestational diabetes mellitus, the mean RFNL thickness was 116µm (*SD* 19) at baseline visit. Since at the time of data evaluation no follow-up measurement was available for the pregnant women with GDM, change in RNFL thickness yet may not be reported. Within the healthy non-pregnant women, the mean RNFL thickness at baseline was 112µm (*SD* 13). At the time of the follow-up visit, the mean RNFL thickness was 110µm (*SD* 13), resulting in a mean descriptive decrease in RNFL thickness of -1.29µm (*SD* 2.72). The corresponding individual descriptive data regarding RNFL thickness is illustrated in table 5.

Table 5

Mean retinal nerve fiber layer thickness across all study groups considering both eyes collectively at baseline and follow-up visit as well as corresponding standard deviations. The change in vessel density was calculated by using the mean of differences.

	Mean			
	Healthy Pregnant (*n* = 2)	**PexD (*n* = 3)**	**GDM (*n* = 8)**	**Healthy non-pregnant (*n* = 38)**
Baseline RNFL thickness (in µm)	102 (1)	109 (11)	116 (19)	112 (13)
Follow-up RNFL thickness (in µm)	100 (6)	110 (14)		110 (13)
Change in RNFL thickness (in µm)	-1.50 (4.95)	0.67 (3.06)		-1.29 (2.72)

3.2.4. Retinal vessel density: Superficial Capillary Plexus (SCP)

The retinal vessel density of the superficial capillary plexus (SCP), the deep capillary plexus (DCP) as well as the radial peripapillary capillary plexus (RPCP) is analyzed descriptively for the whole macula as well as specifically the foveal region. Again, except for the pregnant women with gestational diabetes mellitus, data from both visits is reported, but inferential statistical analyses are omitted due to the limitations in data mentioned before. As mentioned before, in analogy to previous literature, the evaluation of vessel density of all three vascular plexuses is performed across both eyes in total. The change in vessel density for all three plexuses is reported in absolute terms, indicating a direct total change based on the mean of differences rather than a percentage change. While the mean vessel density of the superficial capillary plexus within the healthy pregnant women was 50.3% (*SD* 3.6) in whole macula at the time of the baseline visit, it measured 50.7% (*SD* 0.6) at the time of the follow-up visit. This equates to an absolute mean descriptive increase in vessel density of 0.40% (*SD* 3.09). In the fovea, the mean vessel density was 18.8% (*SD* 6.0) at the time of the baseline visit whereas it was 19.1% (*SD* 3.3) at the time of follow-up. As the mean change between baseline and follow-up visits is calculated based on the mean of the differences, a mean increase in foveal SCP vessel density of 0.30% (*SD* 2.66) is descriptively observed. Within the pregnant women with preexisting diabetes mellitus, the mean SCP vessel density of the whole macula at weeks 25 – 28 of gestation was 51.1% (*SD* 1.8). In weeks 37 – 40 of gestation it was 51.6% (*SD* 2.0). Based on the mean of differences, this equals a mean descriptive increase in vessel density of 0.53% (*SD* 2.07). Regarding the fovea, the mean SCP vessel density was 18.1% (*SD* 4.1) at the time of the baseline visit. At follow-up, it measured 20.1% (*SD* 4.5), resulting in a mean increase of foveal SCP vessel density of 2.02% (*SD* 2.77). In the pregnant women with gestational diabetes mellitus, at the time of baseline visit, a mean SCP vessel density of 48.0% (*SD* 3.6) for the whole macula and 23.6% (*SD* 7.5) for the fovea was observed. As at the time of data evaluation no data of the second visit was available for the pregnant women with gestational diabetes, a mean change in vessel density cannot be reported. Regarding the whole macula, at the time of the baseline visit, a mean vessel density of 50.7% (*SD* 2.1) was observed within the healthy non-pregnant women. At follow-up, the mean SCP vessel density was 51.0% (*SD* 2.8). Thus, a mean descriptive increase in SCP vessel density of 0.29% (*SD* 2.54) was observed. Regarding the fovea, the mean SCP vessel density was 23.8% (*SD* 6.9) at baseline and 24.0% (SD

6.8) at the time of follow-up. This corresponds to a mean increase of foveal SCP vessel density of 0.23% (*SD* 1.93).

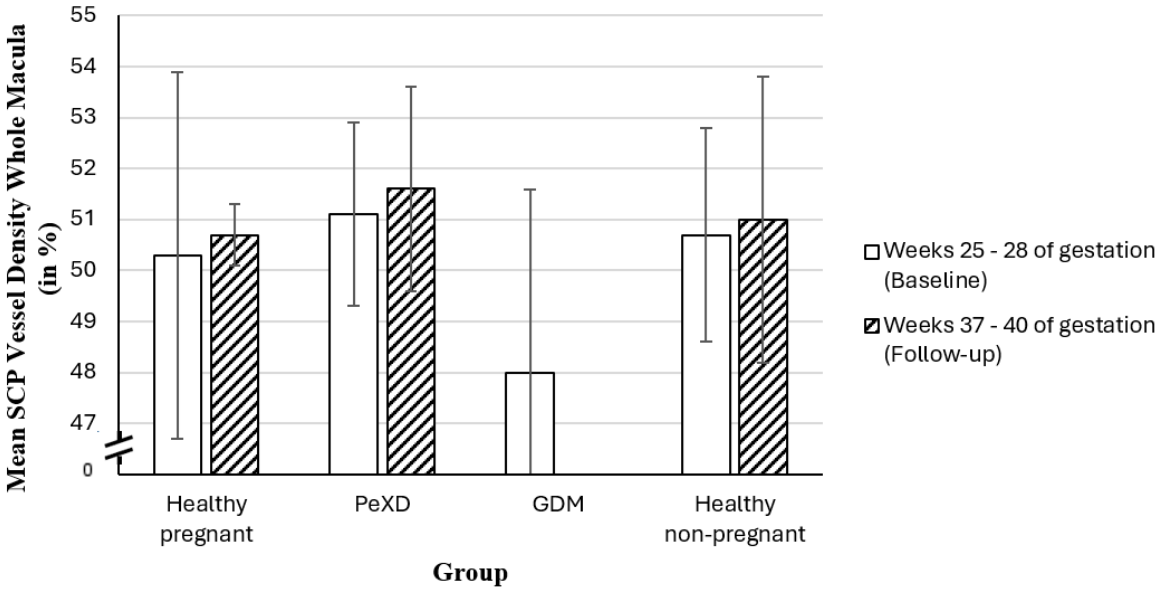

Figure 8. Mean SCP vessel density for the whole macula (in %) considering both eyes collectively across all four groups at baseline and at follow-up visits. The standard deviation is presented as error bars.

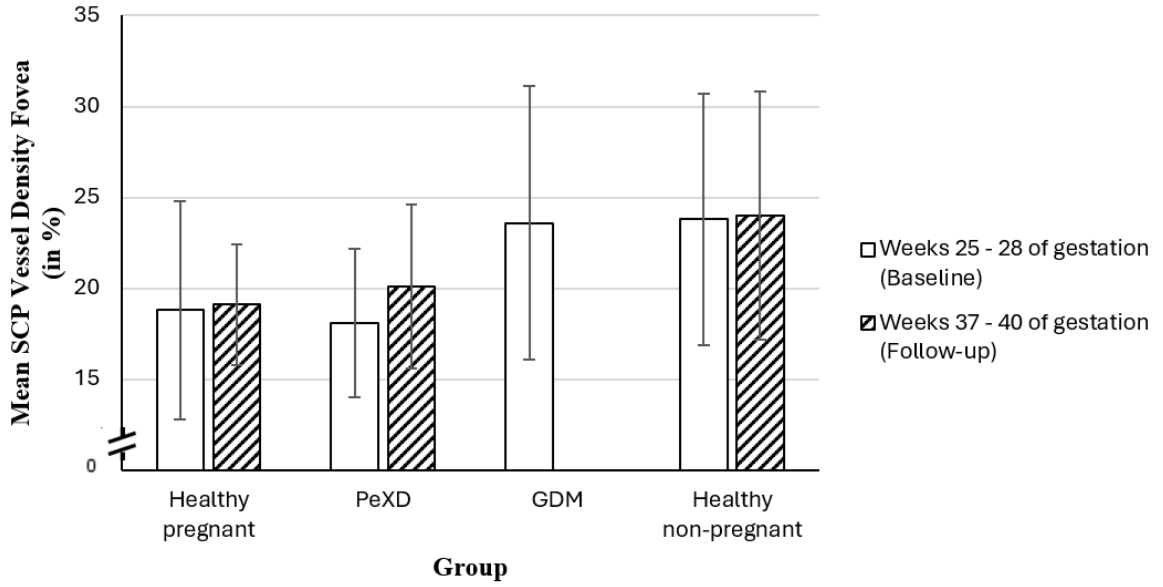

Figure 9. Mean SCP vessel density for the fovea (in %) considering both eyes collectively across all four groups at baseline and at follow-up visits. The standard deviation is presented as error bars.

For further illustration, the descriptive mean values regarding SCP vessel density across both eyes in total are shown in table 6.

Table 6

Mean vessel density of the superficial capillary plexus in percent across all study groups considering both eyes collectively at baseline and follow-up visit as well as corresponding standard deviations. The change in vessel density was calculated by using the mean of differences.

		Mean			
		Healthy Pregnant (*n* = 4)	**PexD (*n* = 11)**	**GDM (*n* = 8)**	**Healthy non-pregnant (*n* = 36)**
Baseline SCP Density (in %)	Whole Macula	50.3 (3.6)	51.1 (1.8)	48.0 (3.6)	50.7 (2.1)
	Fovea	18.8 (6.0)	18.1 (4.1)	23.6 (7.5)	23.8 (6.9)
Follow-Up SCP Density (in %)	Whole Macula	50.7 (0.6)	51.6 (2.0)		51.0 (2.8)
	Fovea	19.1 (3.3)	20.1 (4.5)		24.0 (6.8)
Change in SCP Density (in %)	Whole Macula	0.40 (3.09)	0.53 (2.07)		0.29 (2.54)
	Fovea	0.30 (2.66)	2.02 (2.77)		0.23 (1.93)

3.2.5. Retinal vessel density: Deep Capillary Plexus (DCP)

As for the superficial capillary plexus, changes in vessel density of the deep capillary plexus will not be analyzed by using inferential statistics but will instead be reported and discussed descriptively.

Within the healthy pregnant women, a mean vessel density of the deep capillary plexus of 49.0% (*SD* 6.0) in the whole macula was observed at the time of the baseline visit. At follow-up, the DCP vessel density was 56.2% (*SD* 7.3), descriptively indicating in a mean increase in DCP vessel density of 7.17% (*SD* 2.35) calculated on the mean of differences. For the fovea, the mean vessel density was 37.3% (*SD* 5.5) at baseline and 38.5% (*SD* 2.1) at follow-up. Thus, a mean descriptive increase of 1.25% (*SD* 3.55) in foveal DCP vessel density was observed. In the women with preexisting diabetes mellitus, the whole macula DCP vessel density was 52.6% (*SD* 4.9) at the time of baseline visit and 54.5% (*SD* 5.3) at the time of follow-up. Overall, a mean descriptive increase in vessel density of 1.92% (*SD* 4.64) was observed. Regarding the fovea, the mean DCP vessel density was 37.0% (*SD* 4.0) at baseline visit and 37.2% (*SD* 4.2) at the time of follow-up. Based on the mean of

differences, this corresponds to a mean increase in foveal DCP vessel density of 0.21% (*SD* 1.19). Within the pregnant women with gestational diabetes mellitus, the mean vessel density of DCP was 50.2% (*SD* 5.8) in the whole macula and 41.0% (*SD* 8.2) in the fovea. As at the time of data analysis none of the women with GDM have yet undergone the follow-up examination, no mean change in vessel density may be reported. In the healthy non-pregnant women, regarding the whole macula, a mean DCP vessel density of 51.2% (*SD* 6.0) was observed at the time of the baseline visit. At follow-up, the vessel density measured 51.9% (*SD* 6.3). Descriptively, a mean increase in DCP vessel density of 0.71% (*SD* 5.28) was observed. For the fovea, the mean vessel density of DCP was 40.5% (*SD* 7.4) at the time of the baseline visit, and 41.1% (*SD* 7.0) at follow-up. This equals to a mean descriptive increase of foveal DCP vessel density of 0.62% (*SD* 2.63) based on the mean of differences.

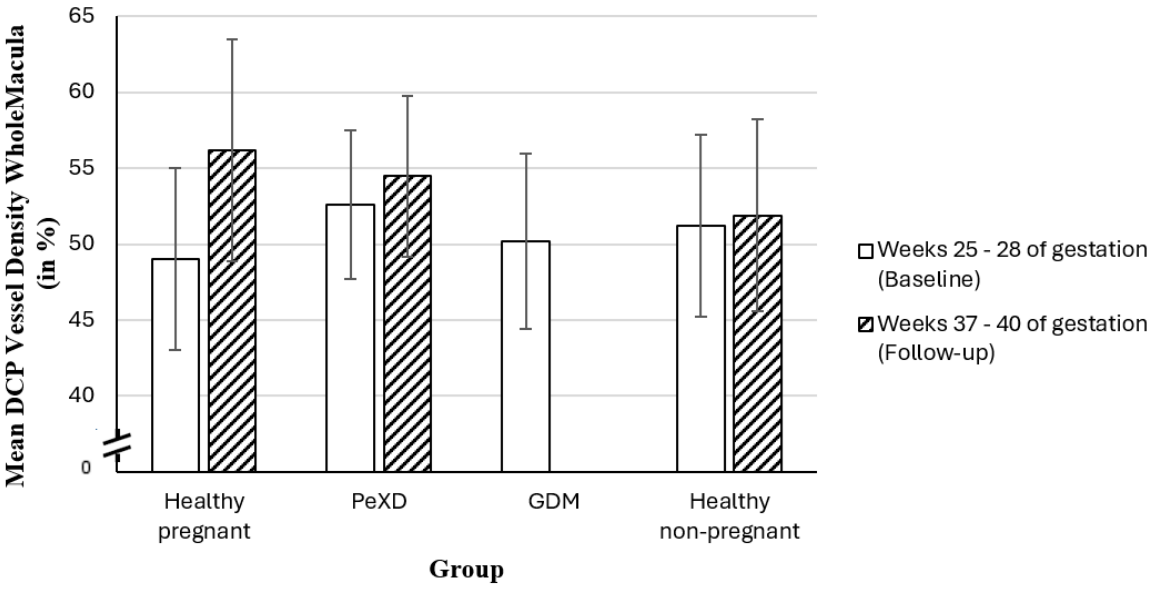

Figure 10. Mean DCP vessel density for the whole macula (in %) considering both eyes collectively across all four groups at baseline and at follow-up visits. The standard deviation is presented as error bars.

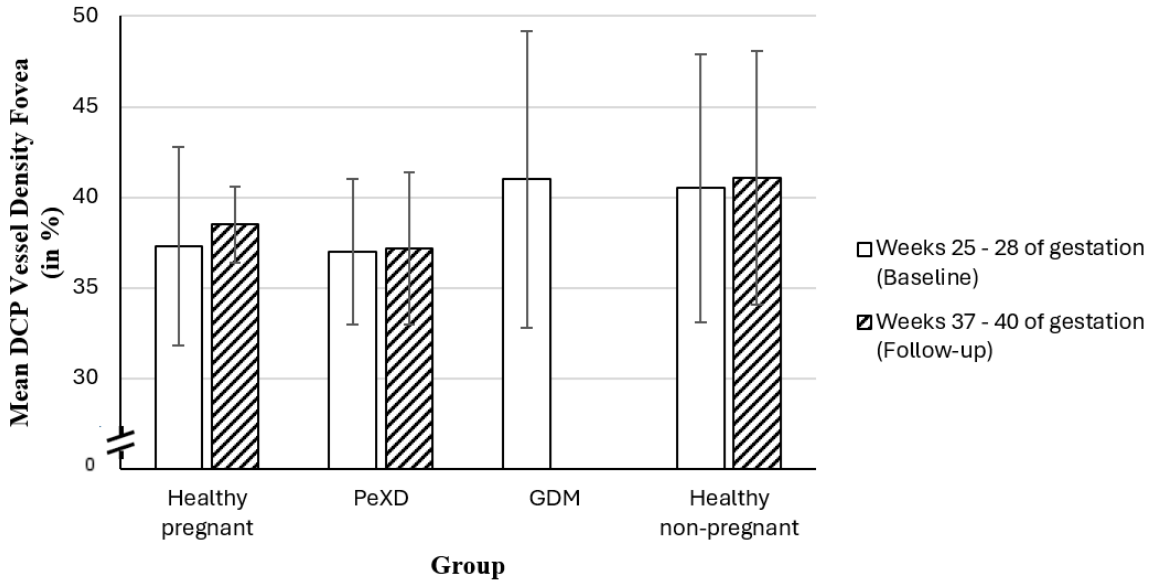

Figure 11. Mean DCP vessel density for the fovea (in %) considering both eyes collectively across all four groups at baseline and at follow-up visits. The standard deviation is presented as error bars.

Respective descriptive data regarding DCP vessel density considering both eyes collectively are shown in table 7.

Table 7

Mean vessel density of the deep capillary plexus in percent across all study groups considering both eyes collectively at baseline and follow-up visit as well as corresponding standard deviations. The change in vessel density was calculated by using the mean of differences.

		Mean			
		Healthy Pregnant (*n* = 4)	**PexD (*n* = 11)**	**GDM (*n* = 8)**	**Healthy non-pregnant (*n* = 35)**
Baseline DCP Density (in %)	Whole Macula	49.0 (6.0)	52.6 (4.9)	50.2 (5.8)	51.2 (6.0)
	Fovea	37.3 (5.5)	37.0 (4.0)	41.0 (8.2)	40.5 (7.4)
Follow-Up DCP Density (in %)	Whole Macula	56.2 (7.3)	54.5 (5.3)	/	51.9 (6.3)
	Fovea	38.5 (2.1)	37.2 (4.2)	/	41.1 (7.0)
Change in DCP Density (in %)	Whole Macula	7.17 (2.35)	1.92 (4.64)	/	0.71 (5.28)
	Fovea	1.25 (3.55)	0.21 (1.19)	/	0.62 (2.63)

3.2.6. Small vessel density: Peripapillary Capillary Plexus (RPCP)

The evaluation of vessel density of the radial peripapillary capillary plexus considering both eyes collectively showed a mean vessel density of 52.3% (*SD* 1.1) within the healthy pregnant women at the time of the baseline visit. At the time of follow-up, the mean vessel density was 52.3% (*SD* 2.5). With a mean descriptive change in vessel density of <0.01% (*SD* 1.41), a constant ratio of RPCP vessel density was thus observed within the healthy pregnant women at baseline and at follow-up. In the pregnant women with preexisting diabetes mellitus, the mean RPCP vessel density was 50.1% (*SD* 1.8) at the time of the baseline visit and 49.6% (*SD* 1.7) at the time of follow-up. This equals to a mean decrease of RPCP vessel density of -0.50% (*SD* 0.95). Examining the RPCP vessel density within the pregnant women with gestational diabetes mellitus, the mean vessel density was 54.4% (*SD* 2.8) at the time of baseline. As with the SCP and DCP, the evaluation of mean change in vessel density for the pregnant women with GDM is currently not available, as none of the women with GDM have yet undergone the follow-up measurement. Within the healthy non-pregnant women, at the time of the baseline visit, a mean RPCP vessel density of 52.9% (*SD* 2.4) was observed. At the time of follow-up, the mean vessel density measured 52.5% (*SD* 3.1), whereby a mean descriptive decrease of RPCP vessel density -0.42% (*SD* 2.19) was observed.

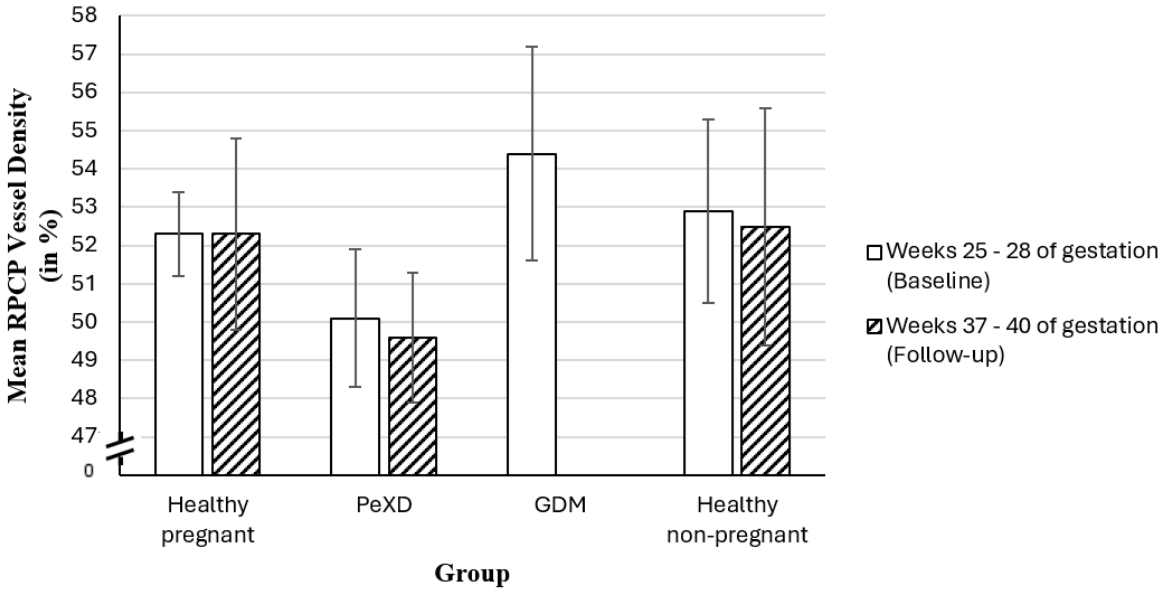

Figure 12. Mean RPCP vessel density (in %) considering both eyes collectively across all four groups at baseline and at follow-up visits. The standard deviation is presented as error bars.

The descriptive data regarding RPCP vessel density across both eyes in total is presented in table 8.

Table 8

Mean small vessel density of the radial peripapillary capillary plexus in percent across all study groups considering both eyes collectively at baseline and follow-up visit as well as corresponding standard deviations. The change in vessel density was calculated by using the mean of differences.

	Mean			
	Healthy Pregnant (*n* = 2)	**PexD (*n* = 3)**	**GDM (*n* = 8)**	**Healthy non-pregnant (*n* = 38)**
Baseline RPCP density (in %)	52.3 (1.1)	50.1 (1.8)	54.4 (2.8)	52.9 (2.4)
Follow-Up RPCP density (in %)	52.3 (2.5)	49.6 (1.7)		52.5 (3.1)
Change in RPCP density (in %)	0.01 (1.41)	-0.50 (0.95)		-0.42 (2.19)

3.2.7. Foveal Avascular Zone (FAZ) size

In the healthy pregnant women, the mean size of the foveal avascular zone at the time of the baseline visit was 0.265mm^2 (*SD* 0.078). At the time of the follow-up visit, the mean size of the FAZ was 0.265mm^2 (*SD* 0.078). Descriptively, considering the mean of differences, no change in FAZ size within the healthy pregnant women was observed. In the pregnant women with preexisting diabetes mellitus, the mean size of the FAZ at weeks 25 – 28 of gestation was 0.283mm^2 (*SD* 0.054). At the time of the follow-up visit at weeks 37 – 40 of gestation, the mean size of the FAZ was 0.277mm^2 (*SD* 0.065). Again, the mean descriptive change in FAZ size in the right eye corresponded to an almost negligible decrease of less than -0.01mm^2 (*SD* 0.02) in the pregnant women with preexisting diabetes mellitus. Within the women with gestational diabetes mellitus, at the time of the baseline visit, the mean size of the FAZ was 0.205mm^2 (*SD* 0.100). Since the follow-up examination had not yet been completed at the time of data evaluation, no data regarding the size of FAZ at a later stage in pregnancy can be provided. Within the healthy non-pregnant women, the mean size of the FAZ at the time of the baseline visit was 0.236mm^2

(*SD* 0.101). At the time of the follow-up visit, the mean size of the FAZ was 0.235mm^2 (*SD* 0.102). Again, descriptively, with an increase of less than <0.001mm^2 (*SD* 0.02), almost no change in mean FAZ size was observed within the healthy non-pregnant women. The respective descriptives are presented in Table 9.

Table 9

Mean size of the foveal avascular zone across all study groups considering both eyes collectively at baseline and follow-up visit as well as corresponding standard deviations. The change in vessel density was calculated by using the mean of differences.

	Mean			
	Healthy Pregnant (*n* = 4)	**PexD (*n* = 11)**	**GDM (*n* = 8)**	**Healthy non-pregnant (*n* = 37)**
Baseline FAZ size (in mm^2)	0.265 (0.078)	0.283 (0.054)	0.205 (0.100)	0.236 (0.101)
Follow-up FAZ size (in mm^2)	0.265 (0.078)	0.277 (0.065)		0.235 (0.102)
Change in FAZ size (in mm^2)	0 (0)	-0.01 (0.02)		<0.001 (0.02)

4. Discussion

The following chapter aims to recapitulate the results obtained, their alignment in the context of current literature as well as discuss substantive methodological strengths and weaknesses, further allowing these insights to be applied within the course of the study. Considering the descriptive change in vessel density of the superficial capillary plexus, an apparent increase, both over the entire macular area as well as specifically for the foveal area across the three observed groups was identified. Although this observation yet lacks statistical confirmation, it entails that the increase in SCP vessel density over the course of pregnancy, between weeks 25 – 28 and weeks 37 – 40 of gestation had a tendency of being greater in pregnant women with and without diabetes mellitus than in healthy non-pregnant controls. As this may indeed imply that pregnancy itself affects retinal vasculature, Kızıltunç et al. (2020) found that vessel density of SCP and DCP, regarding the whole macula, was significantly higher in pregnant women than it was in non-pregnant women. In contrast to the data evaluated, they were able to determine a lower vessel density in the foveal SCP in pregnant women. As with the SCP, the DCP too showed an increase in descriptive values of vessel density in whole macula as well as the foveal area across the three groups evaluated. Regarding the whole macula, again, the increase in vessel density between the time of the baseline visit and the follow-up had a tendency of being greater in the pregnant women than in the non-pregnant controls. To provide a possible explanation, it has to be considered that pregnancy is mostly associated with an increase in blood flow and vascular dilation. This mechanism is hypothesized to be caused primarily due to the production of relaxin, a pregnancy peptide hormone stimulating the formation of endothelin, further mediating vasodilation via nitric oxide synthesis, with studies showing that relaxin deficient mice tend to have normal retinal and choroidal morphology and thickness (Hampel et al., 2020). Additionally, during pregnancy, estrogen, progesterone, and especially renin-angiotensin levels increase significantly, stimulating the synthesis of nitric oxide and further contributing to increased vasodilation and a decrease in peripheral resistance (Chanwimol et al., 2019, Irani & Xia, 2011). As retinal vasculature produces and expresses angiotensin II receptors, local angiotensin II signaling and potential autoregulation of neurovascular activity, increasingly present in pregnancy, occurs (Senanayake et al., 2007). This vasodilation during pregnancy together with the increase in plasma volume of about 50% between weeks of gestation 6 – 32 may be causative for the increase in SCP and DCP density, as suggested by our preliminary data. Regarding the

SCP and DCP vessel density, due to the lack of inferential statistical evaluations, a precise analysis of differences between the four individual groups is currently not permissible. Conclusions regarding a differing affection of vascular plexus density between healthy pregnant women, pregnant women with diabetes mellitus and healthy non-pregnant women have still to be drawn in future data evaluations. The evaluation of the radial peripapillary capillary plexus vessel density revealed a rather heterogeneous pattern, as it showed a decrease within the healthy non-pregnant controls as well as the pregnant women with preexisting diabetes mellitus, while there tended to be no change in vessel density within the healthy pregnant women. As this may presumably be due to- and confounded by the small sample size and the comparatively large SD value, this also needs to be further analyzed in the future in order obtain more reliable results. Interestingly, concurrent descriptive decreases in retinal nerve fiber layer thickness were observed over the time of pregnancy within both healthy pregnant women and healthy non-pregnant women. Although without inferential statistical analyses, currently no conclusions regarding potential differences in RPCP vessel density and RNFL thickness between the four groups may be drawn, these results tend to go in line with those by Mase et al. (2016), who were able to identify a positive correlation between the vessel density of the RPCP and the RNFL thickness.

Regarding the foveal avascular zone, from a solely descriptive perspective, there was almost no change in size of the foveal avascular zone across the three observed groups. These results may be in line with the observations made by Chanwimol et al. (2019) and Hepokur et al. (2021), whereby the size of the FAZ did not differ between pregnant women and non-pregnant women and also remained stable over the course of pregnancy.

Regarding the foveal retinal thickness, compared to the initial retinal thickness at baseline visit at weeks 25 – 28 of gestation, only a slight descriptive change in absolute numbers was seen across the three observed groups over the course of pregnancy, as current values seem to show a tendency for retinal thickness to be particularly stable. While Cankaya et al. (2013) found out that pregnancy itself may indeed affect retinal thickness as they observed an increase in retinal thickness in the second as well as the last trimester of pregnancy using by only optical coherence tomography, the present study can be used to address the lack of sufficient scientific evaluations of retinal thickness over the course of pregnancy as well as between pregnant women with and without diabetes mellitus and non-pregnant women, even using OCTA. For now, additional inferential statistical analyses are required to draw more conclusive results. In contrast, the choroidal thickness

appears to express a more differing pattern. Descriptively, choroidal thickness seems to show higher tendencies of fluctuation within pregnant women with and without diabetes mellitus compared to healthy non-pregnant women. As it should be noted that respective samples, especially those of the healthy pregnant women, are rather small and accompanied by rather high standard deviations within the different groups, these results are to be considered preliminary. A study conducted by Acmaz et al. (2015) found that choroidal thickness indeed was significantly thicker in healthy pregnant women as well as in pregnant women with gestational diabetes mellitus than it was in non-pregnant women, but no difference between healthy pregnant women and pregnant women with diabetes mellitus was reported (Acmaz et al., 2015: 1763). It therefore remains to be seen whether and to what extend said differences are of actual relevance for pregnant women with different forms of diabetes mellitus.

Upon conducting an initial interim analysis of data collected so far, several deficiencies as well as numerous strengths can be derived. To date, the most limiting aspect regarding data acquisition and evaluation is the small sample size, particularly among pregnant women, as several reasons may account for this. While the overall recruitment process initially started back in October 2022, the recruitment of pregnant women with gestational diabetes mellitus was delayed by the Department of Obstetrics and Gynecology because of organizational reasons, causing the first women with gestational diabetes mellitus to complete their baseline examination from mid-May to mid-June of 2023. Unfortunately, the single available AngioVue^{TM} OCT-angiography device failed out of order from mid-July of 2023 to mid-December of 2023, preventing any further tests from being completed during this time. As at said time, the pregnant women with gestational diabetes mellitus would have had the respective follow-up examinations, which were therefore unable to be performed. Overall, a considerable amount of potential participants was lost during this period, what further restricted the sample size. Additionally, the potential ophthalmologic testing of the pregnant women timewise follows as a part of the gynecological or endocrinological examination visits at the clinic, for which the pregnant women may have already stayed in hospital for up to a few hours. Additionally, for the pregnant women with gestational diabetes mellitus, the initial diagnosis is usually first obtained as part of the oral glucose tolerance testing in weeks 24 – 28 of gestation, just before the scheduling of the first baseline visit. This proximity in time as well as the potential impact of the newly obtained diagnosis may thoroughly contribute to the pregnant women's decision to participate in the study. Consequently, the sample size of $n = 16$ for each group,

recommended by the previously performed sample size, was missed. Although the descriptives indeed do indicate a trend over time, statistical conclusions, especially regarding the differences between the four individual groups have to be performed at a later point in time as part of the ongoing study project, as a merely descriptive approach must be currently preferred, at the expense of unrestrained interpretability of data. As the AngioVue™ device has already resumed operation, allowing further testing to continue, while recruitment of all groups has also been resumed, said issues could be expected to be resolved in the near future. While previous literature was often limited to the examination of only a single form of diabetes mellitus in pregnant women, the current study comprehensively includes women with preexisting types of diabetes mellitus as well as gestational diabetes mellitus, allowing more precise comparisons to be made in between the groups. With the inclusion of healthy pregnant women as well as non-pregnant controls, inferential conclusions regarding pregnancy exclusively become possible and by including and evaluating all three vascular plexuses at the same time, even more diverse information on potential vascular affection across the entire retinal microstructure can be provided. Certainly, the foremost strength of the study comes from its longitudinal experimental design, allowing to collect and evaluate consecutive data over time for one and the same cohort. Ultimately, in view of the current indicative descriptive results, a subsequent statistical evaluation remains promising and will soon be following.

References

Acmaz, G., Atas, M., Gulhan, A. *et al*. (2015). Assessment of macular peripapillary nerve fiber layer and choroidal thickness changes in pregnant women with gestational diabetes mellitus, healthy pregnant women and healthy non-pregnant women. *Med Sci Monit*. 2015;21:159-1764

American Diabetes Association. (2021). 2. Classification and diagnosis of diabetes. Standards of Medical Care in Diabetes – 2021. *Diabetes Care*, 2021;44(Suppl. 1):S15-S33. https://doi.org/10.2337/dc21-S002

Aumann, S., Donner, S., Fischer, J. *et al.* (2019). Optical Coherence Tomography (OCT): Principle and Technical Realization. In Bille, J.F. (Ed.). *High Resolution Imaging in Microscopy and Ophthalmology: New Frontiers In Biomedical Optics* (pp. 59-85). Cham: Springer Verlag

Berufsverband der Augenärzte Deutschlands e.V. (2017). Stellungnahme des BVA, der DOG und der RG: OCT-Angiographie in Deutschland. *Der Ophthalmologe*, 114(5), 432-438. https://doi.org/10.1007/s00347-017-0485-z

Böhm, F. (2019). Vergleich und Beurteilung der retinalen Perfusion bei Patienten mit retinalen Venenverschlüssen mit zwei unterschiedlichen Diagnostikverfahren. (Dissertation, Universität Ulm). https://d-nb.info/1233737422/34

Bondello, F., Parodi, M. B., Lanzetta, P. *et al.* (2017). Diabetic Macular Edema. Developments in Ophthalmology. 2017:58:102-138. https://doi.org/10.1159/000455277

Campbell, J.P., Zhang, M., Hwang, T.S., *et al*. (2017). Detailed Vascular Anatomy of the Human Retina by Projection-Resolved Optical Coherence Tomography Angiography. *Nature: Scientific Reports*, 7(1):42201, http://dx.doi.org/10.1038/srep42201

Cankaya, C., Bozkurt, M. & Ulutas, O. (2013). Total Macular Volume and Foveal Retinal Thickness Alterations in Healthy Pregnant Women. *Seminars in Ophthalmology*. 28(2),103-111. https://doi.org/10.3109/08820538.2012.760628

Chanwimol, K., Balasubramanian, S., Nassisi, M. *et al*. (2019). Retinal Vascular Changes During Pregnancy Detected With Optical Coherence Tomography Angiography. *Investigative ophthalmology & visual science*, 60(7). https://doi.org/10.1167/iovs.19-26956

Coscas, F., Glacet-Bernhard, A., Miere, A. *et al.* (2016). Optical Coherence Tomography Angiography in Retinal Vein Occlusion: Evaluation of Superficial and Deep Capillary Plexa. *Americal Journal of Ophthalmology*, 161(pp.160-171)E2, https://doi.org/10.1016/j.ajo.2015.10.008

De Carlo, T. E., Romano, A., Waheed, N. K. *et al*. (2015). A review of optical coherence tomography angiography (OCTA). *International Journal of Retina and Vitreous*, 1,5. https://doi.org/10.1186/s40942-015-0005-8

Deutsche Diabetes Gesellschaft & Deutsche Gesellschaft für Gynäkologie und Geburtshilfe: S3-Leitlinie Gestationsdiabetes mellitus (GDM), Diagnostik, Therapie und Nachsorge (2. Auflage, AWMF-Registernummer: 057-008). (2018). https://register.awmf.org/assets/guidelines/057-008l_S3_Gestationsdiabetes-mellitus-GDM-Diagnostik-Therapie-Nachsorge_2019-06.pdf

Eyefox. (2023). *Optovue XR-Avanti OCT*. https://www.eyefox.com/produkt/1614/optovue-xr-avanti-oct.html (Accessed: 01 March 2023)

Gardner, D.G. & Shoback, D. (2018). *Greenspan's Basic & Clinical Endocrinology*. (10th ed.). McGraw-Hill Education

German Diabetes Association: Clinical Practice Guidelines. (2021). Diabetes and Pregnancy. *Experimental & Clinical Endocrinology and Diabetes*, 129(S 01): S1-S8. https://doi.org/10.1055/a-1284-5758

German Diabetes Association: Clinical Practice Guidelines. (2021). Diabetic Retinopathy and Maculopathy. *Experimental & Clinical Endocrinology and Diabetes*, 129(S 01): S64-S69. https://doi.org/10.1055/a-1284-6223

German Diabetes Association: Clinical Practice Guidelines. (2018). Gestational Diabetes Mellitus (GDM) – Diagnosis, Treatment and Follow-Up. Guideline of the DDG and DGGG (S3 Level, AWMF Registry Number 057/008, February 2018). https://doi.org/10.1055%2Fa-0659-2596

German Diabetes Association: Clinical Practice Guidelines. (2022). Definition, Classification and Diagnosis of Diabetes Mellitus. *Experimental & Clinical Endocrinology and Diabetes*, 130(S 01): S1-S8. https://doi.org/10.1055/a-1624-2897

German Medical Association, German Diabetes Association, German Society of Ophthalmology. (2015). Nationale VersorgungsLeitlinie: Prävention und Therapie von Netzhautkomplikationen bei Diabetes – Langfassung, 2. Auflage Version 2. 2015. AWMF-Registry Number nvl-001b. http://doi.org/10.6101/AZQ/000318

Gervasio, K., & Peck, T. (Eds.). (2022). *The Wills Eye Manual*. (8th ed.). Philadelphia, PA: Wolters Kluwer Health.

Grehn, F. (2019). *Augenheilkunde*. (32nd ed.). Berlin: Springer Verlag *https://*doi*.org/*10.1007/978-3-662-59154-3

Hammes, H.P., Lemmen, K.D. & Bertram, B. (2020). Diabetic Retinopathy and Maculopathy. *Experimental & Clinical Endocrinology and Diabetes,* 129(S 01);S64-S.69. https://doi.org/10.1055/a-1284-6223

Hampel, U., Holly, R., Chinnery, F.G. *et al.* (2020). Ocular Phenotype of Relaxin Gene Knockout ($Rln^{-/-}$) Mice. *Current Eye Research*, 45:10, 1211-1221. https://doi.org/10.1080/02713683.2020.1737714

Harris, A., Guidoboni, G., Siesky, B. *et al*. (2020). Ocular blood flow as a clinical observation: Value, limitations and data analysis. *Progress in Retinal and Eye Research*. Jan 24:100841. https://doi.org/10.1016/j.preteyeres.2020.100841

Heimann, H., Kellner, U. & Foerster, M.H. (2004). *Angiographie-Atlas des Augenhintergrundes*. Stuttgart: Georg Thieme Verlag

Hepokur, M., Busenur, G., Hamzaoglu, K. *et al.* (2021). Investigation of Retinal Vascular Changes during Pregnancy Using Optical Coherence Tomograph Angiography. *Seminars in Ophthalmology*, 36:1-2, 19-27, https://doi.org/10.1080/08820538.2021.1884268

International Diabetes Federation. IDF Diabetes Atlas. (10th ed.). Brussels, Belgium: International Diabetes Federation, 2021. Available at: https://www.diabetesatlas.org

Irani, R.A., Xia, Y. (2011). Renin angiotensin signaling in normal pregnancy and preeclampsia. *Seminars in Nephrology*. 2011, 31:47-58. https://doi.org/10.1016/j.semnephrol.2010.10.005

Kim, A.Y., Chu, Z., Shahidzadeh, A. *et al.* (2016) Quantifying microvascular density and morphology in diabetic retinopathy using spectral-domain optical coherence tomography angiography. Inve*stigative Ophthalmology & Visual Science,* 2016;57(9):OCT 362–70, https://doi.org/10.1167/iovs.15-18904

Kızıltunç, P.B., Varlı, B., Büyüktepe, T.C. & Atilla, H. (2019). Ocular vascular changes during pregnancy: an optical coherence tomography angiography study. *Graefes archive for clinical and experimental Ophthalmology*, 258(2):395-401. https://doi.org/10.1007/s00417-019-04541-6

Ki-Yup, N., Min-Woo, L., Kook-Hyung, L. *et al*. (2022). Superficial capillary plexus vessel density / deep capillary plexus vessel density ratio in healthy eyes. *BMC Ophthalmology*. 22:482. https://doi.org/10.1186/s12886-022-02673-8

Kleinwechter, H., Schäfer-Graf, U., Bührer, C. *et al*. (2021). Diabetes and Pregnancy. *Experimental & Clinical Endocrinology and Diabetes*, 129(S 01):S1-S8. https://doi.org/10.1055/a-1284-5758

Lang, G.E., Enders, C., Werner, J.U. (2016). Neue Möglichkeiten in der retinalen Diagnostik mittels OCT-Angiografie. *Klinische Monatsblätter für Augenheilkunde*. Stuttgart: Georg Thieme Verlag. https://doi.org/10.1055/s-0042-105325

Lemmen, K.D., Agostini, H., Bertram, B. *et al*. (2021). Stadieneinteilung und Therapie der diabetischen Retinopathie und Makulopathie – eine Übersicht. *Zeitschrift für praktische Augenheilkunde & Augenärztliche Fortbildung*, 42: 457-467 (2021).

Linderman, R., Salmon, A.E., & Strampe, M. *et al.* (2017). Assessing the Accuracy of Foveal Avascular Zone Measurements Using Optical Coherence Tomography Angiography: Segmentation and Scaling. *Translational vision science & technology.* 2017;6(3):16. https://doi.org/10.1167/tvst.6.3.16

Löwen, J. (2017, November 21). OCT-Angiographie – Möglichkeiten und Grenzen, *Optometrie*, https://www.doz-verlag.de/Newsbeitrag/oct-angiographie-moeglichkeiten-und-grenzen

Liu, G. & Wang, F. (2021). Macular vascular changes in pregnant women with gestational diabetes mellitus by optical coherence tomography angiography. *BMC Ophthalmology*, 21(1):170. https://doi.org/10.1186/s12886-021-01927-1

Mase, T., Ishibazawa, A., Nagaoka, T. et al. (2016). Radial Peripapillary Capilary Network Visualized Using Wide-Field Montage Optical Coherence Tomography Angiography. *Investigative Opththalmology & Visual Science*, Vol.57: OCT504-OCT510. https://doi.org/10.1167/iovs.15-18877

Medicines.org, SERB. (2018, January 16). *Fluorescein sodium 100mg/ml, solution for injection*, Summary of Product Characteristics, https://www.medicines.org.uk/emc/product/8829/smpc/print (Accessed: 01 March 2023)

Morrison, J.L., Hodgson, L., Lim, L.L. & Al-Qureshi, S. (2016). Diabetic retinopathy in pregnancy: a review. *Clinical & experimental Ophthalmology*, 44(4):321-34. https://doi.org/10.1111/ceo.12760

Musat, O., Cernat, C., Labib, M. *et al.* (2015). Diabetic macular edema. *Romanian Journal of Ophthalmology*. 59(3), Jul-Sep 2015. pp:133-136

Neelakshi, B., Grigorian, R.A., Tutela, A. (2009). Diabetic Macular Edema: Pathogenesis and Treatment. Survey of Ophthalmology, 54(1), 1-32. https://doi.org/10.1016/j.survophthal.2008.10.001

Noctor, E., Dunne, F.P. (2015). Type 2 diabetes after gestational diabetes: The influence of changing diagnostic criteria. *World Journal of Diabetes*, 6(2): 234-244. https://doi.org/10.4239%2Fwjd.v6.i2.234

O'Keefe, G.D. American Academy of Ophthalmology, Eye-Wiki. (2022). Optical Coherence Tomography Angiography. *OCT angiogram of a normal eye illustrating detailed microvasculature in the macula*. Retrieved February 24th, 2023. https://eyewiki.aao.org/w/images/1/thumb/b/be/Normal_OCT_Angiogram_%28Zeiss%29.png/411px-Normal_OCT_Angiogram_%28Zeiss%29.png

Olk, R.J., Halperin, L.S., Soubrane, G. & Coscas, G. (1991). Fluorescein angiography – Is it safe to use in a pregnant patient?. *European Journal of Ophthalmology* 1(2). https://doi.org/10.1177/112067219100100209

Rabbani, N., Thornalley, P.J. (2021). Protein glycation – biomarkers of metabolic dysfunction and early-stage decline in health in the era of precision medicine. *Redox Biology*, Jun;42:101920. https://doi.org/10.1016/j.redox.2021.101920

Senanayake, P., Drazba, J. & Shadrach, K. (2007). Angiotensin II and its receptor subtypes in the human retina. *Investigative ophthalmology and visual science*. Jul;48(7):3301-11. https://doi.org/10.1167/iovs.06-1024

Schmetterer, L., Kiel, J.W. (Eds.). (2012). *Ocular Blood Flow*. (1st ed.). Heidelberg, Berlin: Springer Verlag. https://doi.org/10.1007/978-3-540-69469-4

Silbernagl, S., Lang, F. (2020). Taschenatlas Pathophysiologie. (6th ed.). Stuttgart, New York: Georg Thieme Verlag. https://doi.org/10.1055/b-007-168903

Sugimoto, M., Wakamatsu, Y., Miyata, R. et al. (2019). Relationship between Size of the Foveal Avascular Zone and Carbohydrate Metabolic Disorders during Pregnancy. *BioMed Research International*, 2019:3261279. https://doi.org/10.1155/2019/3261279

University of IOWA Health Care. Department of Ophthalmology and Visual Sciences. (n.d.). Fluorescein Angiography. *Normal Fluorescein Angiogram. Ealy venous phase*. Retrieved February 24th, 2023. https://medicine.uiowa.edu/eye/sites/medicine.uiowa.edu.eye/files/wysiwyg_uploads/FA_Fig2%281%29.jpg (Accessed: 24 February 2023)

Vujosevic, S., Martini, F., Cavarzeran, F. *et al.* (2012) Macular and peripapillary choroidal thickness in diabetic patients. *Retina*, 2012; 32:1781-90. https://doi.org/10.1097/IAE.0b013e31825db73d

Werner, J.U., Böhm, F., Lang, G.E. *et al*. (2019). Comparison of foveal avascular zone between optical coherence tomography angiography and fluorescein angiography in patients with retinal vein occlusion. *PLoS One*. Jun 4;14(6):e0217849. https://doi.org/10.1371/journal.pone.0217849

Wright, P.H., Khalid, H. & Keane, P.A. (2022). The utility of wide-field optical coherence tomography angiography in diagnosis and monitoring of proliferative diabetic retinopathy in pregnancy. *American Journal of Ophthalmology Case Reports* 25(10). https://doi.org/10.1016/j.ajoc.2022.101280

Yanoff, M., Duker, J. (2019). *Ophthalmology*. (5th ed.). Elsevier – Saunders, Mosby, Churchill

Yanuzzi, L.A., Rohrer, K.T., Tindel, L.J. *et al*. (1986). Fluorescein Angiography Complication Survey. *Ophthalmology*, 93(5):611-7. https://doi.org/10.1016/S0161-6420(86)33697-2